

## A SHAPE HESSIAN-BASED BOUNDARY ROUGHNESS ANALYSIS OF NAVIER–STOKES FLOW\*

SHAN YANG<sup>†</sup>, GEORG STADLER<sup>†</sup>, ROBERT MOSER<sup>‡</sup>, AND OMAR GHATTAS<sup>§</sup>

**Abstract.** The influence of boundary roughness characteristics on the rate of dissipation in a viscous fluid is analyzed using shape calculus from the theory of optimal control of systems governed by partial differential equations. To study the mapping  $\mathcal{D}$  from surface roughness topography to the dissipation rate of a Navier–Stokes flow, expressions for the shape gradient and Hessian are determined using the velocity method. In the case of Couette and Poiseuille flows, a flat boundary is a local minimum of the dissipation rate functional. Thus, for small roughness heights the behavior of  $\mathcal{D}$  is governed by the flat-wall shape Hessian operator, whose eigenfunctions are shown to be the Fourier modes. For Stokes flow, the shape Hessian is determined analytically and its eigenvalues are shown to grow linearly with the wavenumber of the shape perturbation. For Navier–Stokes flow, the shape Hessian is computed numerically, and the ratio of its eigenvalues to those of a Stokes flow depend only on the Reynolds number based on the wavelength of the perturbation. The consequences of these results on the analysis of the effects of roughness on fluid flows are discussed.

**Key words.** roughness, Navier–Stokes flow, shape gradient, shape Hessian

**AMS subject classifications.** 35Q30, 65K10, 49Q10, 49Q12

**DOI.** 10.1137/100796789

**1. Introduction.** The flow of fluids over solid surfaces is a common feature of engineered systems. The analysis and control of such fluid flows is complicated by the fact that the surfaces involved are generally rough at some scale. This surface topography can have a significant effect on the rate of momentum transfer to the surface, i.e., on drag. In engineering analysis, the effect of roughness has long been accounted for through the use of empirical adjustments to smooth-wall relations. It is currently not possible to determine these effects directly from a description of the roughness topography. However, predicting and understanding how the characteristics of roughness affect fluid dynamics is important for effective engineering design and analysis.

Generally, the magnitude of the roughness effect on a fluid flow varies with the height of the roughness scaled by the thickness of the fluid shear layer in which it exists. In engineered systems, for which surfaces are made to be relatively smooth, these roughness effects are important in two situations: in lubrication applications, where a thin viscous fluid film flows between sliding surfaces, and in turbulent flows, where the turbulence acts to produce a thin viscously dominated layer very close to the wall (this is the so-called viscous sublayer). As a first step in analyzing the effects of roughness topography, we consider here the effects of roughness in the limit of

---

\*Received by the editors May 28, 2010; accepted for publication (in revised form) December 6, 2010; published electronically February 24, 2011. This work was partially supported by DOE grant DE-FC02-06ER25782 and NSF grants OPP-0941678 and CCF-0427985.

<http://www.siam.org/journals/siap/71-1/79678.html>

<sup>†</sup>Institute for Computational Engineering and Sciences, The University of Texas at Austin, Austin, TX 78712 (syang@ices.utexas.edu, georgst@ices.utexas.edu).

<sup>‡</sup>Institute for Computational Engineering and Sciences and Department of Mechanical Engineering, The University of Texas at Austin, Austin, TX 78712 (rmoser@ices.utexas.edu).

<sup>§</sup>Institute for Computational Engineering and Sciences, Department of Mechanical Engineering, and Department of Geological Sciences, The University of Texas at Austin, Austin, TX 78712 (omar@ices.utexas.edu).

small roughness height for simplified flows that serve as models for the lubrication and turbulence situations.

In the lubrication case, the Reynolds number is generally low, and, in many cases, the flow can be modeled as steady. Thus, the Stokes equations or the steady low Reynolds number Navier–Stokes equations provide a good model for studying roughness effects for lubrication flows.

In turbulent flows, the Reynolds number of the flow as a whole is high, but the relevant feature of the flow is the viscous sublayer, and the Reynolds number of this layer, based on its thickness and the velocity at its edge, is always small, independent of the flow Reynolds number. This occurs because the viscous layer becomes thinner as the Reynolds number increases. Turbulent flows are also unsteady, but the unsteadiness in the viscous sublayer is driven by turbulence farther away from the wall, which is on time scales that are larger than the viscous time scale that governs sublayer dynamics. Thus, as a first approximation, a roughness analysis in the steady low Reynolds number Navier–Stokes equations serves as a model for the turbulent case. A more sophisticated analysis for finite roughness height in (unsteady) turbulent flows is also of great interest but is beyond the scope of this paper. In particular, phenomena such as drag reduction caused by riblets [8, 30] cannot be addressed using the current analysis.

In this paper we focus on Stokes and steady low Reynolds number Navier–Stokes flows. The influence of roughness on drag is studied by analyzing the functional mapping roughness topography to the dissipation rate, which is related to drag through a global energy balance (see section 3). This functional, which we refer to as the *roughness functional* in the remainder of this paper, is given by

$$(1.1) \quad \mathcal{D}(\Omega) = \frac{\nu}{4} \int_{\Omega} (\nabla \mathbf{u} + \nabla \mathbf{u}^T) : (\nabla \mathbf{u} + \nabla \mathbf{u}^T) \, d\mathbf{x},$$

where  $\Omega \subset \mathbb{R}^N$  ( $N = 2, 3$ ) is a domain with a rough boundary surface,  $\nu$  denotes the kinematic viscosity, and  $\mathbf{u}$  is that velocity field that satisfies the stationary incompressible Navier–Stokes equations,

$$(1.2) \quad \begin{aligned} -\nabla \cdot (-Ip + \nu(\nabla \mathbf{u} + \nabla \mathbf{u}^T)) + \mathbf{u} \cdot \nabla \mathbf{u} &= \mathbf{f} & \text{in } \Omega, \\ \nabla \cdot \mathbf{u} &= 0 & \text{in } \Omega, \end{aligned}$$

together with appropriate boundary conditions (to be specified later). The focus of this paper is twofold. First, expressions for the shape derivative and shape Hessian of  $\mathcal{D}$  for general boundary roughness are derived. Second, these expressions are evaluated for a perfectly flat boundary and used in a Taylor expansion to study  $\mathcal{D}$  for small roughnesses. The dependence of the drag increments on the viscosity  $\nu$  and on the characteristics of (small) boundary perturbations are then analyzed.

A common approach to analyzing flow over rough boundaries is to homogenize the roughness to find effective boundary conditions (or a rough wall law) to be applied in a smoother domain; see, e.g., [1, 20, 22]. Parameters in the resulting Robin-type boundary conditions are usually derived numerically from the solution of problems on representative cutouts of the domain. The homogenized problem, which uses the effective boundary conditions, is solved on a smooth domain, and the solution is considered as an approximation to the rough wall flow. In lubrication problems, it is common to homogenize the simpler Reynolds lubrication equation as an alternative to the Navier–Stokes equations [3, 4, 24]. The Reynolds equation is derived as an

asymptotic approximation valid for geometric variations that occur over distances that are large compared to the thickness of the lubrication film. Since roughness geometries commonly vary over small length scales, the validity of roughness homogenization of the Reynolds equation is limited. Generally, the homogenization approach applies for a given roughness or a given type of roughness, and it is unclear how to use it to compute sensitivities with respect to the shape variations to which the drag is most sensitive. Our approach is significantly different from homogenization since we measure the drag directly through the roughness functional (1.1) and consider the shape as a variable. This allows first- and second-order derivative information to be obtained, which is an attractive feature of the shape calculus-based approach for the analysis of flow over rough surfaces.

In the past, shape Hessians (i.e., second-order shape derivatives) have been used mainly as a tool to analyze the well-posedness of shape optimization problems [5, 6, 11, 16]. More recently, approximations of shape Hessians have also been used to accelerate convergence of iterative methods for the solution of shape optimization problems, for example, in imaging [17], aerodynamic design [13, 25], and elliptic shape optimization problems [11, 12].

The tools of shape calculus are reviewed briefly in section 2 and are used in section 3 to derive the shape gradient and Hessian of the roughness functional. Results of this analysis are applied to Couette and Poiseuille flow problems in section 4, and the implications for the fluid mechanics of rough surfaces are discussed in section 5.

**2. Preliminaries.** In this section basic results from shape calculus are recalled, providing a general framework for the computation of first- and second-order shape derivatives (section 2.1). Furthermore, when the shape derivatives are to be taken in the presence of equality constraints, in this case imposed by the Navier–Stokes equations, it is convenient to use the Lagrange method to incorporate the constraints. This approach is outlined in section 2.2.

**2.1. Shape gradients and shape Hessians.** We use the *velocity method* (see [7, 10, 26, 31]) for the computation of shape derivatives, as summarized below. Let  $D \subset \mathbb{R}^N$  be open and  $\Omega \subset D$ . We consider perturbations  $\Omega_t(\mathbf{V}) \subset D$  of  $\Omega$  defined through a perturbation of identity, i.e.,

$$\Omega_t(\mathbf{V}) = \{\mathbf{x} + t\mathbf{V}(\mathbf{x}); \mathbf{x} \in \Omega\}, \quad |t| \leq t_o,$$

where  $\mathbf{V}$  is a Lipschitz continuous velocity field.<sup>1</sup> Let  $\mathcal{J}(\cdot) : \Omega_t(\mathbf{V}) \rightarrow \mathbb{R}$  be a functional; then  $\mathcal{J}$  is said to have a *Hadamard semiderivative* at  $\Omega$  in direction  $\mathbf{V}$  if the limit

$$d\mathcal{J}(\Omega; \mathbf{V}) := \lim_{t \rightarrow 0} \frac{\mathcal{J}(\Omega_t(\mathbf{V})) - \mathcal{J}(\Omega)}{t} = \left. \frac{d}{dt} \mathcal{J}(\Omega_t) \right|_{t=0}$$

exists and is finite.

For later use, we now give derivatives for two shape functionals.

**LEMMA 2.1.** *Let  $\Omega \subset D$  be a bounded and measurable domain and  $\mathbf{V}(\mathbf{x})$  a Lipschitz continuous velocity field. Then, for  $\psi \in W^{1,1}(D) \cap L^1(D)$ ,  $\phi \in H^2(D)$ , the derivatives of the shape functionals,*

$$\mathcal{I}(\Omega_t(\mathbf{V})) = \int_{\Omega_t(\mathbf{V})} \psi \, d\mathbf{x}, \quad \mathcal{J}(\Omega_t(\mathbf{V})) = \int_{\partial\Omega_t(\mathbf{V})} \phi \, d\mathbf{s},$$

<sup>1</sup>Note that the velocity field discussed here is a velocity associated with the continuous transformation of the solution domain in pseudotime  $t$ . It should not be confused with the fluid velocity  $\mathbf{u}$ .

are given by

$$(2.1) \quad d\mathcal{I}(\Omega; \mathbf{V}) = \frac{d}{dt} \mathcal{I}(\Omega_t) \Big|_{t=0} = \int_{\partial\Omega} \psi \mathbf{V} \cdot \mathbf{n} \, ds,$$

$$(2.2) \quad d\mathcal{J}(\Omega; \mathbf{V}) = \frac{d}{dt} \mathcal{J}(\Omega_t) \Big|_{t=0} = \int_{\partial\Omega} (\nabla\phi \cdot \mathbf{n} + H\phi) \mathbf{V} \cdot \mathbf{n} \, ds,$$

where  $H$  is the mean curvature of the boundary and  $\mathbf{n}$  is the unit outward normal vector of  $\partial\Omega$ .

A detailed proof in a more general setting, which is based on a change of variables and the chain rule, can be found, e.g., in [10, pp. 352–355]. Now, for  $\mathbf{g} \in W^{2,1}(D) \cap H^1(D)$ , consider the shape functional

$$\mathcal{K}(\Omega_t(\mathbf{V})) = \int_{\partial\Omega_t(\mathbf{V})} \mathbf{g} \cdot \mathbf{n} \, ds.$$

Using Lemma 2.1, the shape derivative of  $\mathcal{K}$  is

$$(2.3) \quad \begin{aligned} d\mathcal{K}(\Omega; \mathbf{V}) &= \frac{d}{dt} \mathcal{K}(\Omega_t) \Big|_{t=0} = \frac{d}{dt} \left( \int_{\partial\Omega_t(\mathbf{V})} \mathbf{g} \cdot \mathbf{n} \, ds \right) \Big|_{t=0} \\ &= \frac{d}{dt} \left( \int_{\Omega_t(\mathbf{V})} \nabla \cdot \mathbf{g} \, dx \right) \Big|_{t=0} \stackrel{(\text{using (2.1)})}{=} \int_{\partial\Omega} \nabla \cdot \mathbf{g} \mathbf{V} \cdot \mathbf{n} \, ds, \end{aligned}$$

in which the boundary integral is transformed into an integral over the domain  $\Omega$  so that (2.1) can be applied. This technique is also useful for the derivation of second-order shape derivatives, which are based on a second transformation of the domain  $\Omega_t(\mathbf{V})$ , namely, on

$$\Omega_{t,r}(\mathbf{V}, \mathbf{W}) = \{\mathbf{x} + t\mathbf{V}(\mathbf{x}) + r\mathbf{W}(\mathbf{x} + t\mathbf{V}(\mathbf{x})); \mathbf{x} \in \Omega\}, \quad |t| \leq t_0, \quad |r| \leq r_0,$$

where  $\mathbf{V}$  and  $\mathbf{W}$  denote sufficiently smooth velocity fields. The second-order shape derivative of a functional  $\mathcal{J}$  is then defined by

$$d^2 \mathcal{J}(\Omega; \mathbf{V}, \mathbf{W}) = \frac{\partial}{\partial r} \left( \frac{\partial}{\partial t} \mathcal{J}_{\mathbf{V}, \mathbf{W}}(t, r) \Big|_{t=0} \right) \Big|_{r=0}.$$

For  $f \in H^2(D)$ , consider the functional

$$\mathcal{J}_{\mathbf{V}, \mathbf{W}}(t, r) = \mathcal{J}(\Omega_{t,r}(\mathbf{V}, \mathbf{W})) := \int_{\Omega_{t,r}(\mathbf{V}, \mathbf{W})} f \, dx.$$

Using the expression for shape gradients,

$$\frac{\partial}{\partial t} \mathcal{J}_{\mathbf{V}, \mathbf{W}}(t, r) \Big|_{t=0} = d\mathcal{J}(\Omega_r(\mathbf{W}); \mathbf{V}) = \int_{\partial\Omega_r(\mathbf{W})} f \mathbf{V} \cdot \mathbf{n}_r \, ds,$$

where here  $\mathbf{n}_r$  is the outward normal vector of  $\partial\Omega_r$ . Using (2.3), the second shape derivative is given by

$$(2.4) \quad \begin{aligned} d^2 \mathcal{J}(\Omega; \mathbf{V}, \mathbf{W}) &= \frac{d}{dr} \left( \int_{\partial\Omega_r(\mathbf{W})} f \mathbf{V} \cdot \mathbf{n}_r \, ds \right) = \frac{d}{dr} \left( \int_{\Omega_r(\mathbf{W})} \nabla \cdot (f \mathbf{V}) \, dx \right) \\ &= \int_{\partial\Omega} \nabla \cdot (f \mathbf{V})(\mathbf{W} \cdot \mathbf{n}) \, ds. \end{aligned}$$

Naturally, the following question arises: Under which conditions is the shape Hessian symmetric? As shown in [10], a sufficient condition for the shape Hessian to be symmetric is that the velocity fields  $\mathbf{V}$  and  $\mathbf{W}$  satisfy

$$(2.5) \quad \int_{\partial\Omega} f((\nabla\mathbf{V})\mathbf{W} - (\nabla\mathbf{W})\mathbf{V}) \cdot \mathbf{n} \, ds = 0 \quad \text{for all } f \in C^2(D).$$

Note that in the shape derivative formulae stated here in (2.1)–(2.4), the derivatives are expressed in terms of boundary integrals involving  $\mathbf{V}$  and  $\mathbf{W}$ , so that the shape perturbations matter only in a neighborhood of the boundary  $\partial\Omega$ .

**2.2. The formal Lagrange method.** We seek the shape derivatives in the presence of an equality constraint (here the Navier–Stokes equations). The constraint can be incorporated using Lagrange multipliers. This approach is outlined below but without concern for the technical details that arise in infinite dimensions (see [9, 15, 19, 21, 29] for a more complete treatment). We are interested in the derivative of a functional  $J(q, u)$  with respect to a *control variable*  $q$ , in which the *state variable*  $u$  depends implicitly on  $q$  through a *state equation*  $c(q, u) = 0$ :

$$(2.6) \quad \begin{aligned} \hat{J}: \quad q &\longmapsto J(q, u) \\ \text{subject to} \quad c(q, u) &= 0. \end{aligned}$$

Here,  $\hat{J}$  incorporates the dependence of the state  $u$  on the control  $q$  via the solution of  $c(q, u) = 0$ ; in other words,  $\hat{J}(q) := J(q, u(q))$ .

Introducing the Lagrange multiplier (also known as the *adjoint state variable*)  $\lambda$ , the *Lagrangian functional* is defined by

$$\mathcal{L}(q, u, \lambda) = J(q, u) + (c(q, u), \lambda),$$

where  $(\cdot, \cdot)$  denotes an appropriate inner product. The gradient of the Lagrangian functional is given by

$$\begin{bmatrix} \delta_u \mathcal{L} \\ \delta_q \mathcal{L} \\ \delta_\lambda \mathcal{L} \end{bmatrix} := \begin{bmatrix} \delta_u J + c_u^* \lambda \\ \delta_q J + c_q^* \lambda \\ c \end{bmatrix},$$

where  $\delta_u \mathcal{L}$ ,  $\delta_q \mathcal{L}$  are the variations of the Lagrangian with respect to  $u$  and  $q$ , respectively, and analogously for  $\delta_u J$  and  $\delta_q J$ , and the dependence of all operators on  $q$  and  $u$  has been suppressed for notational simplicity. Moreover,  $c_u$  and  $c_q$  are the Jacobians of the state equations with respect to the state and control variables, respectively, and  $c_u^*$  and  $c_q^*$  denote the adjoint operators. The *reduced gradient*  $d\hat{J}/dq$  is then given simply by  $\delta_q \mathcal{L}$  evaluated for values of  $u$  and  $\lambda$  such that the *adjoint equation*  $\delta_u \mathcal{L} = 0$  and the *state equation*  $\delta_\lambda \mathcal{L} = 0$  are satisfied.

The reduced gradient can thus be determined by the following procedure:

1. Given  $q$ , solve the state equation  $c = 0$  for  $u$ .
2. Given  $q$  and  $u$ , solve the adjoint equation  $\delta_u J + c_u^* \lambda = 0$  for  $\lambda$ .
3. Given  $q$ ,  $u$ , and  $\lambda$ , evaluate the reduced gradient  $d\hat{J}/dq = \delta_q J + c_q^* \lambda$ .

The *reduced Hessian*  $d^2\hat{J}/dq^2$  can be determined by finding the Schur complement of the control block in the matrix of second variations of  $\mathcal{L}$  with respect to  $(u, q, \lambda)$ , i.e., in the matrix

$$\begin{bmatrix} \delta_{uu}^2 \mathcal{L} & \delta_{uq}^2 \mathcal{L} & c_u^* \\ \delta_{qu}^2 \mathcal{L} & \delta_{qq}^2 \mathcal{L} & c_q^* \\ c_u & c_q & 0 \end{bmatrix}.$$

Thus,

$$(2.7) \quad \frac{d^2 \hat{J}}{dq^2} = \delta_{qq}^2 \mathcal{L} - \begin{bmatrix} \delta_{qu}^2 \mathcal{L} & c_q^* \\ c_u & 0 \end{bmatrix} \begin{bmatrix} \delta_{uu}^2 \mathcal{L} & c_u^* \\ c_u & 0 \end{bmatrix}^{-1} \begin{bmatrix} \delta_{uq}^2 \mathcal{L} \\ c_q \end{bmatrix},$$

where  $\delta_{uu}^2 \mathcal{L}$  and  $\delta_{uq}^2 \mathcal{L}$  are the variations of  $\delta_u \mathcal{L}$  with respect to  $u$  and  $q$ , respectively, and analogously for  $\delta_{qu}^2 \mathcal{L}$ ,  $\delta_{qq}^2 \mathcal{L}$ . Often, it is not necessary or feasible to fully construct the reduced Hessian. Instead, it suffices to know its action in arbitrary directions. An efficient way to compute the action of the reduced Hessian in a direction  $\hat{q}$  is to introduce auxiliary variables  $\hat{u}, \hat{\lambda}$  defined by

$$(2.8) \quad - \begin{bmatrix} \delta_{uu}^2 \mathcal{L} & c_u^* \\ c_u & 0 \end{bmatrix}^{-1} \begin{bmatrix} \delta_{uq}^2 \mathcal{L} \\ c_q \end{bmatrix} \hat{q} = \begin{bmatrix} \hat{u} \\ \hat{\lambda} \end{bmatrix}.$$

In what follows,  $\hat{u}$  and  $\hat{\lambda}$  are referred to as *incremental state* and *incremental adjoint* variables. Once the state and adjoint equations have been solved, the action of the reduced Hessian in the direction  $\hat{q}$  can be computed as follows:

1. Given  $q, u$ , and  $\hat{q}$ , solve the *incremental state equation* (i.e., the lower equation in (2.8))

$$c_u \hat{u} + c_q \hat{q} = 0 \quad \text{for } \hat{u}.$$

2. Given  $q, u, \lambda, \hat{q}$ , and  $\hat{u}$ , solve the *incremental adjoint equation* (i.e., the upper equation in (2.8))

$$\delta_{uu}^2 \mathcal{L} \hat{u} + c_u^* \hat{\lambda} + \delta_{uq}^2 \mathcal{L} \hat{q} = 0 \quad \text{for } \hat{\lambda}.$$

3. Finally, given  $q, u, \lambda, \hat{q}, \hat{u}, \hat{\lambda}$ , evaluate the action of the reduced Hessian on  $\hat{q}$  by

$$\frac{d^2 \hat{J}}{dq^2} \hat{q} = \delta_{qq}^2 \mathcal{L} \hat{q} + \delta_{qu}^2 \mathcal{L} \hat{u} + c_q^* \hat{\lambda}.$$

Note that the incremental state equation can be viewed as one more variation of  $\delta_\lambda \mathcal{L}$  with respect to all variables; thus, below we will use  $\delta_{\lambda^\bullet}^2$  to denote the residual of the incremental state equation, and analogously  $\delta_{u^\bullet}^2$  for the incremental adjoint equation.

**3. The roughness functional and its shape derivatives.** The shape calculus outlined in section 2 will be applied here to the roughness functional that maps the boundary topography to the drag exerted on fluid flow governed by the Navier–Stokes equations. The resulting expressions for the shape gradient and shape Hessian will be applied in section 4 to analyze the effects of small roughness on an otherwise flat boundary.

**3.1. Problem statement.** Of interest here is the steady incompressible flow of a fluid between two walls (e.g., in a channel), where for simplicity only one wall is rough, as sketched in Figure 3.1. The flow is governed by the incompressible, stationary Navier–Stokes equations,

$$(3.1a) \quad \begin{aligned} -\nabla \cdot (-Ip + \nu(\nabla \mathbf{u} + \nabla \mathbf{u}^T)) + \mathbf{u} \cdot \nabla \mathbf{u} - \mathbf{f} &= \mathbf{0} & \text{in } \Omega, \\ \nabla \cdot \mathbf{u} &= 0 & \text{in } \Omega, \end{aligned}$$

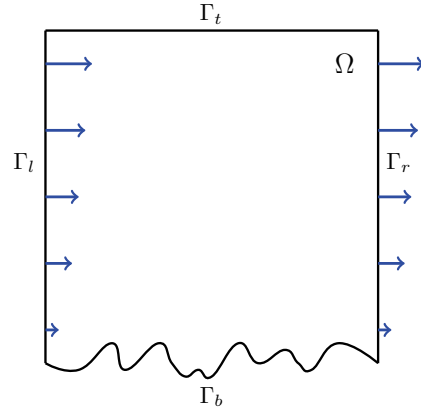


FIG. 3.1. Sketch of domain  $\Omega$  with rough bottom boundary  $\Gamma_b$ . The flow is periodic on the left and right boundaries  $\Gamma_l$  and  $\Gamma_r$ . In three dimensions, the flow is also periodic on the fore and aft boundaries  $\Gamma_f$  and  $\Gamma_a$  (not shown).

on the domain  $\Omega \subset D \subset \mathbb{R}^N$  ( $N = 2, 3$ ). Here,  $\mathbf{u}$  is the flow velocity (which should not be confused with the domain deformation “velocities”  $\mathbf{V}$  and  $\mathbf{W}$ ),  $p$  is the pressure, and  $\mathbf{f}$  is a body force. The latter two variables have been rescaled to eliminate the density. The channel is taken to be infinitely long in the directions parallel to the wall, with roughness topography, boundary condition data, and forcing  $\mathbf{f}$  that are periodic in the streamwise ( $x$ ) and spanwise ( $y$ ) directions with periods  $L_x$  and  $L_y$ , respectively. The solutions we seek are also periodic in both directions with the same periods. Solutions will thus be sought on a domain  $\Omega$  that is finite with periodic boundary conditions in the streamwise and spanwise directions. To be precise, in the case of a three-dimensional domain  $\Omega$  (i.e.,  $N = 3$ ; specialization to  $N = 2$  is obvious) the boundaries in the  $x$  direction (left and right) and the  $y$  direction (fore and aft) are denoted by  $\Gamma_l$ ,  $\Gamma_r$ ,  $\Gamma_f$ , and  $\Gamma_a$ , respectively, and the flow velocity  $\mathbf{u}$  as well as the traction  $(-Ip + \nu(\nabla\mathbf{u} + \nabla\mathbf{u}^T)) \mathbf{n}$  (where  $\mathbf{n}$  is the unit outward normal vector) must coincide on  $\Gamma_l$  and  $\Gamma_r$ , and on  $\Gamma_f$  and  $\Gamma_a$ . This, along with  $\nabla \cdot \mathbf{u} = 0$ , implies that  $p$  and  $\nabla\mathbf{u}$  must also coincide on periodic boundaries. For subsequent use, the periodic boundaries are designated collectively as  $\Gamma_p$ , and vector fields such as  $\mathbf{u}$  will simply be described as periodic on  $\Gamma_p$  when these conditions are satisfied. For the bottom and top boundaries  $\Gamma_b$  and  $\Gamma_t$ , respectively, the no-slip boundary condition is imposed, so the velocity is specified as

$$(3.1b) \quad \mathbf{u} = \mathbf{0} \quad \text{on } \Gamma_b,$$

$$(3.1c) \quad \mathbf{u} = \mathbf{u}_0 \quad \text{on } \Gamma_t,$$

where  $\mathbf{u}_0$  is the specified velocity of the upper boundary with  $\mathbf{u}_0 \cdot \mathbf{n} = 0$  on  $\Gamma_t$ .

Our primary interest is the effect of roughness on the drag for a domain with fixed volume. In this context, the drag is simply the driving force required to maintain the steady fluid flow, and it is generally of interest because energy is required to do work on the flow. The rate at which work is done on the flow is thus a particularly relevant measure of the drag phenomenon. Furthermore, in the special cases of Couette flow ( $\mathbf{f} = 0$ ,  $\mathbf{u}_0$  fixed) and Poiseuille flow ( $\mathbf{u}_0 = 0$ , volume flow rate fixed) to be considered in section 4, the drag force is directly proportional to the rate of work. Using the notation  $\boldsymbol{\tau} = -Ip + \nu(\nabla\mathbf{u} + \nabla\mathbf{u}^T)$  for the stress tensor, the total rate of work on the

fluid is given by

$$\begin{aligned}
& \int_{\partial\Omega} \mathbf{u} \cdot (\boldsymbol{\tau} \mathbf{n}) \, ds + \int_{\Omega} \mathbf{u} \cdot \mathbf{f} \, d\mathbf{x} \\
&= \int_{\Omega} \nabla \mathbf{u} : \boldsymbol{\tau} \, d\mathbf{x} + \int_{\Omega} \mathbf{u} \cdot (\nabla \cdot \boldsymbol{\tau} + \mathbf{f}) \, d\mathbf{x} \\
&= \int_{\Omega} \frac{\nu}{2} (\nabla \mathbf{u} + \nabla \mathbf{u}^T) : (\nabla \mathbf{u} + \nabla \mathbf{u}^T) \, d\mathbf{x} + \int_{\Omega} \mathbf{u} \cdot (\mathbf{u} \cdot \nabla \mathbf{u}) \, d\mathbf{x} \\
&= \int_{\Omega} \frac{\nu}{2} (\nabla \mathbf{u} + \nabla \mathbf{u}^T) : (\nabla \mathbf{u} + \nabla \mathbf{u}^T) \, d\mathbf{x}.
\end{aligned}$$

The last equality follows from

$$\int_{\Omega} \mathbf{u} \cdot (\mathbf{u} \cdot \nabla \mathbf{u}) \, d\mathbf{x} = \frac{1}{2} \int_{\partial\Omega} (\mathbf{u} \cdot \mathbf{u}) \mathbf{u} \cdot \mathbf{n} \, ds - \frac{1}{2} \int_{\Omega} (\mathbf{u} \cdot \mathbf{u}) \nabla \cdot \mathbf{u} \, d\mathbf{x} = 0,$$

which holds since  $\mathbf{u} \cdot \mathbf{n} = 0$  on  $\Gamma_b$  and  $\Gamma_t$ ; periodicity holds on  $\Gamma_p$  and  $\nabla \cdot \mathbf{u} = 0$ . Thus, the effect of roughness on the drag is the same as its effect on the rate of kinetic energy dissipation. The roughness functional  $\mathcal{D}$  will be defined using the dissipation form because this is more convenient for the subsequent derivations. Note that to obtain a certain structure of the adjoint Navier–Stokes equations (which will be derived below), the work done by drag is scaled by a factor of  $1/2$  in  $\mathcal{D}$ :

$$(3.2) \quad \mathcal{D}(\Gamma_b) = \frac{\nu}{4} \int_{\Omega} (\nabla \mathbf{u} + \nabla \mathbf{u}^T) : (\nabla \mathbf{u} + \nabla \mathbf{u}^T) \, d\mathbf{x},$$

where  $(\mathbf{u}, p)$  solves (3.1) on  $\Omega$ .

The shape derivatives of the roughness functional  $\mathcal{D}$  can now be derived. Since the roughness functional (3.2) involves the solution of the Navier–Stokes equations, the Lagrangian approach described in section 2.2 is used. For that purpose, the Navier–Stokes equations are written in variational form and treated as equality constraints in appropriate infinite-dimensional spaces. In particular, consider the following subspaces of  $\mathbf{H}^1(\Omega) := (H^1(\Omega))^N$ :

$$\begin{aligned}
\tilde{\mathbf{H}}^1(\Omega) &= \{\mathbf{u} \in \mathbf{H}^1(\Omega) : \mathbf{u} \text{ is periodic on } \Gamma_p\}, \\
\tilde{\mathbf{H}}_{\mathbf{u}_0}^1(\Omega) &= \{\mathbf{u} \in \tilde{\mathbf{H}}^1(\Omega) : \mathbf{u} = \mathbf{u}_0 \text{ on } \Gamma_t\}, \\
\tilde{\mathbf{H}}_0^1(\Omega) &= \{\mathbf{u} \in \tilde{\mathbf{H}}^1(\Omega) : \mathbf{u} = \mathbf{0} \text{ on } \Gamma_t\},
\end{aligned}$$

where  $\mathbf{u}_0 \in \tilde{\mathbf{H}}^1(\Omega)$  with  $\mathbf{u}_0 \cdot \mathbf{n} = 0$  on  $\Gamma_t$ . The variational form of the Navier–Stokes equation is given as follows: Find  $(\mathbf{u}, p) \in \tilde{\mathbf{H}}_{\mathbf{u}_0}^1(\Omega) \times L^2(\Omega)$  such that

$$(3.3) \quad \int_{\Omega} \frac{\nu}{2} (\nabla \mathbf{u} + \nabla \mathbf{u}^T) : (\nabla \mathbf{v} + \nabla \mathbf{v}^T) \, d\mathbf{x} - \int_{\Omega} (q \nabla \cdot \mathbf{u} + p \nabla \cdot \mathbf{v}) \, d\mathbf{x} + \int_{\Omega} (\mathbf{u} \cdot \nabla \mathbf{u}) \cdot \mathbf{v} \, d\mathbf{x} \\
- \int_{\Omega} \mathbf{f} \cdot \mathbf{v} \, d\mathbf{x} + \int_{\Gamma_b} \boldsymbol{\alpha} \cdot \mathbf{u} \, ds = \int_{\Gamma_b} \mathbf{v} \cdot (-Ip + \nu(\nabla \mathbf{u} + \nabla \mathbf{u}^T)) \mathbf{n} \, ds$$

for all  $(\mathbf{v}, q, \boldsymbol{\alpha}) \in \tilde{\mathbf{H}}_0^1(\Omega) \times L^2(\Omega) \times \mathbf{H}^{-1/2}(\Gamma_b)$ . Note that in (3.3) the boundary condition on  $\Gamma_b$  is enforced weakly as this is needed for the computation of shape derivatives. It is well known (see, e.g., [28, p. 67]) that (3.3) admits a solution  $(\mathbf{u}, p) \in$

$\tilde{\mathbf{H}}_{\mathbf{u}_0}^1(\Omega) \times L^2(\Omega)$  for each  $\Omega$  with  $\partial\Omega \in C^{0,1}$  and  $\mathbf{f} \in \mathbf{L}^2(\Omega)$ . Here, higher regularity  $\mathbf{f} \in \tilde{\mathbf{H}}^2(\Omega)$  (i.e.,  $\mathbf{f} \in \mathbf{H}^2(\Omega)$ , and  $\mathbf{f}$  is periodic on  $\Gamma_p$ ) and bounded  $\Omega$  with  $\partial\Omega \in C^{3,1}$  are assumed, to meet requirements for the existence of shape derivatives. Introducing Lagrange multipliers  $\boldsymbol{\lambda} \in \tilde{\mathbf{H}}_0^1(\Omega)$ ,  $\alpha \in L^2(\Omega)$ , and  $\boldsymbol{\beta} \in \mathbf{H}^{-1/2}(\Gamma_b)$ , the Lagrangian functional is defined by

$$\begin{aligned} \mathcal{L}(\Gamma_b, \mathbf{u}, p, \boldsymbol{\lambda}, \alpha, \boldsymbol{\beta}) &= \frac{\nu}{4} \int_{\Omega} (\nabla \mathbf{u} + \nabla \mathbf{u}^T) : (\nabla \mathbf{u} + \nabla \mathbf{u}^T) \, d\mathbf{x} - \int_{\Omega} \alpha \nabla \cdot \mathbf{u} + \nabla \cdot \boldsymbol{\lambda} p \, d\mathbf{x} \\ &\quad + \int_{\Omega} \left( \frac{\nu}{2} (\nabla \boldsymbol{\lambda} + \nabla \boldsymbol{\lambda}^T) : (\nabla \mathbf{u} + \nabla \mathbf{u}^T) + (\mathbf{u} \cdot \nabla \mathbf{u}) \cdot \boldsymbol{\lambda} - \boldsymbol{\lambda} \cdot \mathbf{f} \right) \, d\mathbf{x} \\ &\quad - \int_{\Gamma_b} \boldsymbol{\lambda} \cdot (-Ip + \nu(\nabla \mathbf{u} + \nabla \mathbf{u}^T)) \mathbf{n} \, ds + \int_{\Gamma_b} \boldsymbol{\beta} \cdot \mathbf{u} \, ds. \end{aligned}$$

In the derivations of the shape gradient and shape Hessian,  $\mathbf{u}, p$  are referred to as state variables;  $\boldsymbol{\lambda}, \alpha, \boldsymbol{\beta}$  are referred to as adjoint variables; and the incremental state and incremental adjoint variables are denoted by  $\hat{\mathbf{u}}, \hat{p}, \hat{\boldsymbol{\lambda}}, \hat{\alpha}, \hat{\boldsymbol{\beta}}$ . Finally, test functions in variational formulations are denoted by  $\tilde{\mathbf{u}}, \tilde{p}, \tilde{\boldsymbol{\lambda}}, \tilde{\alpha}, \tilde{\boldsymbol{\beta}}$ .

**3.2. Shape gradient.** As described in section 2.2, determining the gradient of  $\mathcal{D}$  with respect to the shape  $\Omega$  (or equivalently  $\Gamma_b$ ) requires solutions to the state and adjoint equations.

It is easy to see that setting variations of  $\mathcal{L}$  with respect to the Lagrange multipliers to zero results in the weak form (3.3) of the Navier–Stokes equations. Variations with respect to  $\mathbf{u}$  and  $p$  result in the adjoint equations for  $(\boldsymbol{\lambda}, \alpha)$ :

$$\begin{aligned} \delta_{\mathbf{u}} \mathcal{L} &= \int_{\Omega} \left( \frac{\nu}{2} (\nabla \mathbf{u} + \nabla \mathbf{u}^T) : (\nabla \tilde{\mathbf{u}} + \nabla \tilde{\mathbf{u}}^T) + \frac{\nu}{2} (\nabla \boldsymbol{\lambda} + \nabla \boldsymbol{\lambda}^T) : (\nabla \tilde{\mathbf{u}} + \nabla \tilde{\mathbf{u}}^T) \right) \, d\mathbf{x} \\ (3.4a) \quad &- \int_{\Omega} \alpha \nabla \cdot \tilde{\mathbf{u}} \, d\mathbf{x} - \int_{\Gamma_b} \boldsymbol{\lambda} \cdot \nu(\nabla \tilde{\mathbf{u}} + \nabla \tilde{\mathbf{u}}^T) \mathbf{n} \, ds + \int_{\Gamma_b} \boldsymbol{\beta} \cdot \tilde{\mathbf{u}} \, ds \\ &+ \int_{\Omega} (\tilde{\mathbf{u}} \cdot \nabla \mathbf{u} + \mathbf{u} \cdot \nabla \tilde{\mathbf{u}}) \cdot \boldsymbol{\lambda} \, d\mathbf{x} = 0, \end{aligned}$$

(3.4b)

$$\delta_p \mathcal{L} = \int_{\Omega} (-\nabla \cdot \boldsymbol{\lambda}) \tilde{p} \, d\mathbf{x} + \int_{\Gamma_b} \tilde{p} \boldsymbol{\lambda} \cdot \mathbf{n} \, ds = 0$$

for all  $(\tilde{\mathbf{u}}, \tilde{p}) \in \tilde{\mathbf{H}}_0^1(\Omega) \times L^2(\Omega)$ . Integration by parts in (3.4a) yields

$$\begin{aligned} &\int_{\Omega} (-\nabla \cdot (-I\alpha + \nu(\nabla \mathbf{u} + \nabla \mathbf{u}^T) + \nu(\nabla \boldsymbol{\lambda} + \nabla \boldsymbol{\lambda}^T)) + \nabla \mathbf{u}^T \boldsymbol{\lambda} - \nabla \boldsymbol{\lambda} \mathbf{u}) \cdot \tilde{\mathbf{u}} \, d\mathbf{x} \\ &+ \int_{\partial\Omega} (-I\alpha + \nu(\nabla \mathbf{u} + \nabla \mathbf{u}^T) + \nu(\nabla \boldsymbol{\lambda} + \nabla \boldsymbol{\lambda}^T)) \mathbf{n} \cdot \tilde{\mathbf{u}} \, ds + \int_{\Gamma_b} \boldsymbol{\beta} \cdot \tilde{\mathbf{u}} \, ds \\ (3.5) \quad &- \int_{\partial\Omega} (\mathbf{u} \cdot \mathbf{n})(\boldsymbol{\lambda} \cdot \tilde{\mathbf{u}}) \, ds - \int_{\partial\Omega} \boldsymbol{\lambda} \cdot (\nabla \tilde{\mathbf{u}} + \nabla \tilde{\mathbf{u}}^T) \mathbf{n} \, ds = 0. \end{aligned}$$

From the boundary condition for  $\mathbf{u}$ , we conclude that the corresponding strong form of the adjoint equations is given by

$$(3.6a) \quad -\nabla \cdot (-I\alpha + \nu(\nabla \mathbf{u} + \nabla \mathbf{u}^T) + \nu(\nabla \boldsymbol{\lambda} + \nabla \boldsymbol{\lambda}^T)) + \nabla \mathbf{u}^T \boldsymbol{\lambda} - \nabla \boldsymbol{\lambda} \mathbf{u} = \mathbf{0} \quad \text{in } \Omega,$$

$$(3.6b) \quad \nabla \cdot \boldsymbol{\lambda} = 0 \quad \text{in } \Omega,$$

with  $\boldsymbol{\lambda} = 0$  on  $\Gamma_t \cup \Gamma_b$  and periodic on  $\Gamma_p$ . In addition, (3.5) implies that

$$(3.6c) \quad \boldsymbol{\beta} = - \left( -I\alpha + \nu(\nabla \mathbf{u} + \nabla \mathbf{u}^T) + \nu(\nabla \boldsymbol{\lambda} + \nabla \boldsymbol{\lambda}^T) \right) \mathbf{n}.$$

Due to the regularity assumptions on  $\mathbf{f}$  and  $\partial\Omega$ , regularity theory (see, e.g., [27]) yields that  $\mathbf{u} \in \mathbf{H}^4(\Omega) \cap \mathbf{H}_0^1(\Omega)$  and  $p \in H^3(\Omega)$ . Due to our assumption  $\Omega \in C^{3,1}$ ,  $\mathbf{u}$  and  $p$  can be extended to functions in  $\mathbf{H}^4(D)$  and  $H^3(D)$ , respectively (see [14]). Similar results hold for  $\boldsymbol{\lambda}$  and  $\alpha$ , and (3.6c) implies that  $\boldsymbol{\beta} \in \mathbf{H}^3(D)$ . Thus, the integrands in  $\mathcal{L}$  satisfy the requirements of Lemma 2.1, which shows that the Lagrangian  $\mathcal{L}$  is shape differentiable with respect to  $\Gamma_b$ . Additionally, for  $N = 2, 3$ , the Rellich–Kondrachov embedding theorem (see [2, p. 144]) shows that  $\mathbf{f} \in C(\bar{\Omega})$  and  $\mathbf{u} \in C^2(\bar{\Omega})$ , where  $\bar{\Omega}$  is the closure of  $\Omega$ . This regularity result implies that the Navier–Stokes equations are satisfied up to the boundary, which allows certain simplifications of boundary terms.

Next, the velocity method is used to derive the shape derivative in direction  $\mathbf{V}$  via (2.1), (2.2), and (2.3). To apply (2.3) for the computation of the derivative with respect to the shape, the boundary integrals over  $\Gamma_b$  in the Lagrangian functional can be extended to  $\partial\Omega$  if  $\boldsymbol{\beta}$  is extended to  $\Omega$  such that it is periodic on  $\Gamma_p$  and vanishes on  $\Gamma_t$ . Thus, the shape derivative is given by

$$\begin{aligned} & d\mathcal{D}(\Gamma_b; \mathbf{V}) \\ &= \int_{\Gamma_b} \frac{\nu}{4} (\nabla \mathbf{u} + \nabla \mathbf{u}^T) : (\nabla \mathbf{u} + \nabla \mathbf{u}^T) \mathbf{V} \cdot \mathbf{n} \, ds - \int_{\Gamma_b} \alpha \nabla \cdot \mathbf{u} \mathbf{V} \cdot \mathbf{n} \, ds \\ &\quad + \int_{\Gamma_b} \left( -\nabla \cdot \boldsymbol{\lambda} p + \frac{\nu}{2} (\nabla \boldsymbol{\lambda} + \nabla \boldsymbol{\lambda}^T) : (\nabla \mathbf{u} + \nabla \mathbf{u}^T) - \boldsymbol{\lambda} \cdot \mathbf{f} \right) \mathbf{V} \cdot \mathbf{n} \, ds \\ &\quad - \int_{\Gamma_b} \nabla \cdot (\boldsymbol{\lambda} \cdot (-Ip + \nu(\nabla \mathbf{u} + \nabla \mathbf{u}^T))) \mathbf{V} \cdot \mathbf{n} \, ds + \int_{\Gamma_b} (\mathbf{u} \cdot \nabla \mathbf{u}) \cdot \boldsymbol{\lambda} \mathbf{V} \cdot \mathbf{n} \, ds \\ &\quad + \int_{\Gamma_b} \nabla \cdot (-(-I\alpha + \nu(\nabla \mathbf{u} + \nabla \mathbf{u}^T) + \nu(\nabla \boldsymbol{\lambda} + \nabla \boldsymbol{\lambda}^T)) \mathbf{u}) \mathbf{V} \cdot \mathbf{n} \, ds \\ &= \int_{\Gamma_b} \left( \frac{\nu}{4} (\nabla \mathbf{u} + \nabla \mathbf{u}^T) : (\nabla \mathbf{u} + \nabla \mathbf{u}^T) + \frac{\nu}{2} (\nabla \boldsymbol{\lambda} + \nabla \boldsymbol{\lambda}^T) : (\nabla \mathbf{u} + \nabla \mathbf{u}^T) \right) \mathbf{V} \cdot \mathbf{n} \, ds \\ &\quad - \int_{\Gamma_b} (\nabla \mathbf{u} : (\nu(\nabla \mathbf{u} + \nabla \mathbf{u}^T) + \nu(\nabla \boldsymbol{\lambda} + \nabla \boldsymbol{\lambda}^T)) + \nabla \boldsymbol{\lambda} : \nu(\nabla \mathbf{u} + \nabla \mathbf{u}^T)) \mathbf{V} \cdot \mathbf{n} \, ds \\ &\quad + \int_{\Gamma_b} \boldsymbol{\lambda} \cdot (-\nabla \cdot (-Ip + \nu(\nabla \mathbf{u} + \nabla \mathbf{u}^T)) + \mathbf{u} \cdot \nabla \mathbf{u} - \mathbf{f}) \mathbf{V} \cdot \mathbf{n} \, ds \\ &\quad + \int_{\Gamma_b} -\nabla \cdot (-I\alpha + \nu(\nabla \mathbf{u} + \nabla \mathbf{u}^T) + \nu(\nabla \boldsymbol{\lambda} + \nabla \boldsymbol{\lambda}^T)) \cdot \mathbf{u} \mathbf{V} \cdot \mathbf{n} \, ds \\ (3.7) \quad &= \int_{\Gamma_b} \left( -\frac{\nu}{4} (\nabla \mathbf{u} + \nabla \mathbf{u}^T) - \frac{\nu}{2} (\nabla \boldsymbol{\lambda} + \nabla \boldsymbol{\lambda}^T) \right) : (\nabla \mathbf{u} + \nabla \mathbf{u}^T) \mathbf{V} \cdot \mathbf{n} \, ds, \end{aligned}$$

where  $\mathbf{V}$  is the boundary deformation for which the gradient is evaluated, and the regularity properties argued above, as well as the equality

$$\nabla \mathbf{u} : \nu(\nabla \mathbf{u} + \nabla \mathbf{u}^T) = \frac{\nu}{2} (\nabla \mathbf{u} + \nabla \mathbf{u}^T) : (\nabla \mathbf{u} + \nabla \mathbf{u}^T),$$

are used to simplify the expressions. Note that, compared to the approach used in [25], our results for the shape gradient contain additional terms that involve  $\nabla \mathbf{u}^T$  and

$\nabla \boldsymbol{\lambda}^T$ . However, the two expressions can be shown to be equivalent: since  $\mathbf{u}$  vanishes on  $\Gamma_b$ ,  $\nabla \mathbf{u}$  is nonzero only in directions normal to the boundary. The divergence-free condition additionally implies that  $(\mathbf{n} \cdot \nabla \mathbf{u}) \cdot \mathbf{n} = 0$ , which yields that

$$(3.8) \quad \nabla \mathbf{u} : \nabla \mathbf{u}^T = 0 \text{ on } \Gamma_b.$$

Analogously, one may argue that  $\nabla \mathbf{u} : \nabla \boldsymbol{\lambda}^T = 0$ , and thus our results for the gradient are consistent with those in [25]. The findings in this section are summarized in the next theorem.

**THEOREM 3.1.** *The shape gradient of  $\mathcal{D}$  at  $\Omega$  in the direction of the shape velocity field  $\mathbf{V}$  is given by (3.7), where  $(\mathbf{u}, p)$  denote the solution to the state equation (3.1), and  $(\boldsymbol{\lambda}, \alpha)$  denote the solution to the adjoint equations (3.6).*

**3.3. Shape Hessian.** The shape Hessian operator is particularly important at stationary points, where the shape gradient vanishes and the second order derivatives determine the local behavior of the roughness functional. Using the assumptions that  $\mathbf{f} \in \mathbf{H}^2(\Omega)$  and  $\Omega$  is a bounded domain with a  $C^{3,1}$  boundary, we see that  $d\mathcal{D}(\Gamma_b; \mathbf{V})$  as defined in (3.7) is differentiable with respect to  $\Gamma_b$  since the integrands are in  $W^{2,1}(\Omega)$  and can be extended to  $W^{2,1}(D)$ . Hence one more derivative of the Lagrangian functional can be taken to derive the shape Hessian operator. Let  $\mathbf{W}$  be the velocity field corresponding to the second shape variation. Variations of  $\delta_{\boldsymbol{\lambda}} \mathcal{L}$  yield that for all  $\tilde{\boldsymbol{\lambda}} \in \tilde{\mathbf{H}}_0^1(\Omega)$ ,

$$(3.9) \quad \begin{aligned} \delta_{\tilde{\boldsymbol{\lambda}}}^2 \mathcal{D}(\Gamma_b, \mathbf{W}) &= \int_{\Omega} \left( -\nabla \cdot \tilde{\boldsymbol{\lambda}} \hat{p} + \frac{\nu}{2} (\nabla \tilde{\boldsymbol{\lambda}} + \nabla \tilde{\boldsymbol{\lambda}}^T) : (\nabla \hat{\mathbf{u}} + \nabla \hat{\mathbf{u}}^T) \right. \\ &\quad \left. + (\hat{\mathbf{u}} \cdot \nabla \mathbf{u} + \mathbf{u} \cdot \nabla \hat{\mathbf{u}}) \cdot \tilde{\boldsymbol{\lambda}} \right) d\mathbf{x} - \int_{\Gamma_b} \tilde{\boldsymbol{\lambda}} \cdot (-I \hat{p} + \nu (\nabla \hat{\mathbf{u}} + \nabla \hat{\mathbf{u}}^T)) \mathbf{n} ds \\ &\quad + \int_{\Gamma_b} (-\nabla \cdot (-I p + \nu (\nabla \mathbf{u} + \nabla \mathbf{u}^T)) + \mathbf{u} \cdot \nabla \mathbf{u} - \mathbf{f}) \cdot \tilde{\boldsymbol{\lambda}} \mathbf{W} \cdot \mathbf{n} ds. \end{aligned}$$

As introduced in section 2, here  $\delta_{\tilde{\boldsymbol{\lambda}}}^2 \mathcal{L}$  denotes a variation of  $\delta_{\boldsymbol{\lambda}} \mathcal{L}$  with respect to all variables. Using (3.6c), for all  $(\tilde{\boldsymbol{\alpha}}, \tilde{\boldsymbol{\beta}}) \in L^2(\Omega) \times \mathbf{H}^{-1/2}(\Omega)$ ,

$$(3.10) \quad \delta_{\tilde{\boldsymbol{\alpha}}}^2 \mathcal{D}(\Gamma_b, \mathbf{W}) = - \int_{\Omega} \tilde{\boldsymbol{\alpha}} \nabla \cdot \hat{\mathbf{u}} d\mathbf{x} - \int_{\Gamma_b} (\tilde{\boldsymbol{\alpha}} \nabla \cdot \mathbf{u}) \mathbf{W} \cdot \mathbf{n} ds,$$

$$(3.11) \quad \begin{aligned} \delta_{\tilde{\boldsymbol{\beta}}}^2 \mathcal{D}(\Gamma_b, \mathbf{W}) &= \int_{\Gamma_b} \left( -I \tilde{\boldsymbol{\alpha}} + \nu (\nabla \tilde{\mathbf{u}} + \nabla \tilde{\mathbf{u}}^T) + \nu (\nabla \tilde{\boldsymbol{\lambda}} + \nabla \tilde{\boldsymbol{\lambda}}^T) \right) \hat{\mathbf{u}} \cdot \mathbf{n} ds \\ &\quad + \int_{\Gamma_b} \left( -I \tilde{\boldsymbol{\alpha}} + \nu (\nabla \tilde{\mathbf{u}} + \nabla \tilde{\mathbf{u}}^T) + \nu (\nabla \tilde{\boldsymbol{\lambda}} + \nabla \tilde{\boldsymbol{\lambda}}^T) \right) : \nabla \mathbf{u} \mathbf{W} \cdot \mathbf{n} ds \\ &\quad + \int_{\Gamma_b} \nabla \cdot \left( -I \tilde{\boldsymbol{\alpha}} + \nu (\nabla \tilde{\mathbf{u}} + \nabla \tilde{\mathbf{u}}^T) + \nu (\nabla \tilde{\boldsymbol{\lambda}} + \nabla \tilde{\boldsymbol{\lambda}}^T) \right) \cdot \mathbf{u} \mathbf{W} \cdot \mathbf{n} ds. \end{aligned}$$

Setting (3.9) and (3.10) to zero leads to the following strong form for the incremental state equation for  $(\hat{\mathbf{u}}, \hat{p})$ :

$$(3.12) \quad \begin{aligned} -\nabla \cdot (-I \hat{p} + \nu (\nabla \hat{\mathbf{u}} + \nabla \hat{\mathbf{u}}^T)) + \mathbf{u} \cdot \nabla \hat{\mathbf{u}} + \hat{\mathbf{u}} \cdot \nabla \mathbf{u} &= \mathbf{0} \quad \text{in } \Omega, \\ \nabla \cdot \hat{\mathbf{u}} &= 0 \quad \text{in } \Omega, \\ \hat{\mathbf{u}} + (\nabla \mathbf{u} + \nabla \mathbf{u}^T) \mathbf{n} \mathbf{W} \cdot \mathbf{n} &= \mathbf{0} \quad \text{on } \Gamma_b. \end{aligned}$$

Additionally,  $\hat{\mathbf{u}}$  vanishes on  $\Gamma_t$  and is periodic on  $\Gamma_p$ . Next, the incremental adjoint equations are obtained from the variations of  $\delta_u \mathcal{L}$  and  $\delta_p \mathcal{L}$ . From (3.4a), we obtain for all  $(\tilde{\mathbf{u}}, \tilde{p}) \in \tilde{\mathbf{H}}_0^1(\Omega) \times L^2(\Omega)$ ,

$$\begin{aligned}
\delta_{\mathbf{u}\bullet}^2 \mathcal{D}(\Gamma_b, \mathbf{W}) &= \int_{\Omega} \frac{\nu}{2} (\nabla \hat{\mathbf{u}} + \nabla \hat{\mathbf{u}}^T) : (\nabla \tilde{\mathbf{u}} + \nabla \tilde{\mathbf{u}}^T) + \frac{\nu}{2} (\nabla \hat{\boldsymbol{\lambda}} + \nabla \hat{\boldsymbol{\lambda}}^T) : (\nabla \tilde{\mathbf{u}} + \nabla \tilde{\mathbf{u}}^T) \, d\mathbf{x} \\
&\quad - \int_{\Omega} \hat{\alpha} \nabla \cdot \tilde{\mathbf{u}} \, d\mathbf{x} + \int_{\Omega} \left( (\tilde{\mathbf{u}} \cdot \nabla \hat{\mathbf{u}} + \hat{\mathbf{u}} \cdot \nabla \tilde{\mathbf{u}}) \cdot \boldsymbol{\lambda} + (\tilde{\mathbf{u}} \cdot \nabla \mathbf{u} + \mathbf{u} \cdot \nabla \tilde{\mathbf{u}}) \cdot \hat{\boldsymbol{\lambda}} \right) \, d\mathbf{x} \\
&\quad - \int_{\Gamma_b} \left( -I \hat{\alpha} + (\nabla \hat{\mathbf{u}} + \nabla \hat{\mathbf{u}}^T) + (\nabla \hat{\boldsymbol{\lambda}} + \nabla \hat{\boldsymbol{\lambda}}^T) \right) \mathbf{n} \cdot \tilde{\mathbf{u}} \, ds \\
&\quad + \int_{\Gamma_b} \frac{\nu}{2} (\nabla \mathbf{u} + \nabla \mathbf{u}^T + \nabla \boldsymbol{\lambda} + \nabla \boldsymbol{\lambda}^T) : (\nabla \tilde{\mathbf{u}} + \nabla \tilde{\mathbf{u}}^T) \mathbf{W} \cdot \mathbf{n} \, ds \\
(3.13) \quad &\quad - \int_{\Gamma_b} \alpha \nabla \cdot \tilde{\mathbf{u}} \mathbf{W} \cdot \mathbf{n} \, ds + \int_{\Gamma_b} (\tilde{\mathbf{u}} \cdot \nabla \mathbf{u} + \mathbf{u} \cdot \nabla \tilde{\mathbf{u}}) \cdot \boldsymbol{\lambda} \mathbf{W} \cdot \mathbf{n} \, ds \\
&\quad - \int_{\Gamma_b} \nabla \cdot (\boldsymbol{\lambda} \cdot \nu (\nabla \tilde{\mathbf{u}} + \nabla \tilde{\mathbf{u}}^T)) \mathbf{W} \cdot \mathbf{n} \, ds - \int_{\Gamma_b} \hat{\boldsymbol{\lambda}} \cdot \nu (\nabla \tilde{\mathbf{u}} + \nabla \tilde{\mathbf{u}}^T) \mathbf{n} \, ds \\
&\quad - \int_{\Gamma_b} \nabla \cdot \left( (-I \alpha + \nu (\nabla \mathbf{u} + \nabla \mathbf{u}^T) + \nu (\nabla \boldsymbol{\lambda} + \nabla \boldsymbol{\lambda}^T)) \tilde{\mathbf{u}} \right) \mathbf{W} \cdot \mathbf{n} \, ds.
\end{aligned}$$

For all  $\tilde{p} \in L^2(\Omega)$ ,

$$\begin{aligned}
\delta_{p\bullet}^2 \mathcal{D}(\Gamma_b, \mathbf{W}) &= \int_{\Omega} (-\nabla \cdot \hat{\boldsymbol{\lambda}}) \tilde{p} \, d\mathbf{x} + \int_{\Gamma_b} \tilde{p} \hat{\boldsymbol{\lambda}} \cdot \mathbf{n} \, ds + \int_{\Gamma_b} (-\nabla \cdot \boldsymbol{\lambda}) \tilde{p} \mathbf{W} \cdot \mathbf{n} \, ds \\
&\quad + \int_{\Gamma_b} \nabla \cdot (\tilde{p} \boldsymbol{\lambda}) \mathbf{W} \cdot \mathbf{n} \, ds, \\
(3.14) \quad &= \int_{\Omega} (-\nabla \cdot \hat{\boldsymbol{\lambda}}) \tilde{p} \, d\mathbf{x} + \int_{\Gamma_b} \tilde{p} \hat{\boldsymbol{\lambda}} \cdot \mathbf{n} \, ds + \int_{\Gamma_b} \nabla \tilde{p} \cdot \boldsymbol{\lambda} \mathbf{W} \cdot \mathbf{n} \, ds \\
&= \int_{\Omega} (-\nabla \cdot \hat{\boldsymbol{\lambda}}) \tilde{p} \, d\mathbf{x}.
\end{aligned}$$

The variational forms (3.13), (3.14) are equivalent to the following strong form of the incremental adjoint equations:

$$(3.15a) \quad -\nabla \cdot \left( -I \hat{\alpha} + \nu (\nabla \hat{\mathbf{u}} + \nabla \hat{\mathbf{u}}^T) + \nu (\nabla \hat{\boldsymbol{\lambda}} + \nabla \hat{\boldsymbol{\lambda}}^T) \right) = -\nabla \hat{\mathbf{u}}^T \boldsymbol{\lambda} - \nabla \mathbf{u}^T \hat{\boldsymbol{\lambda}} + \nabla \boldsymbol{\lambda} \hat{\mathbf{u}} + \nabla \hat{\boldsymbol{\lambda}} \mathbf{u} \quad \text{in } \Omega,$$

$$(3.15b) \quad \nabla \cdot \hat{\boldsymbol{\lambda}} = 0 \quad \text{in } \Omega,$$

$$(3.15c) \quad \hat{\boldsymbol{\lambda}} + (\nabla \boldsymbol{\lambda} + \nabla \boldsymbol{\lambda}^T) \mathbf{n} (\mathbf{W} \cdot \mathbf{n}) = 0 \quad \text{on } \Gamma_b.$$

Additionally,  $\hat{\boldsymbol{\lambda}} = 0$  on  $\Gamma_t$  and is periodic on  $\Gamma_p$ . Defining  $\mathbf{V}$  and  $\mathbf{W}$  as shape perturbations in the velocity method and using (2.4), we are able to obtain a simplified form for the evaluation of the shape Hessian in directions  $(\mathbf{V}, \mathbf{W})$  since the residuals of the state and adjoint momentum and mass equations on the boundary vanish:

$$\begin{aligned}
 d^2 \mathcal{D}(\Gamma_b; \mathbf{V}, \mathbf{W}) = & \int_{\Gamma_b} \left( -\frac{\nu}{2}(\nabla \mathbf{u} + \nabla \mathbf{u}^T) : (\nabla \hat{\mathbf{u}} + \nabla \hat{\mathbf{u}}^T) - \frac{\nu}{2}(\nabla \boldsymbol{\lambda} + \nabla \boldsymbol{\lambda}^T) : \right. \\
 (3.16) \quad & \left. (\nabla \hat{\mathbf{u}} + \nabla \hat{\mathbf{u}}^T) - \frac{\nu}{2}(\nabla \hat{\boldsymbol{\lambda}} + \nabla \hat{\boldsymbol{\lambda}}^T) : (\nabla \mathbf{u} + \nabla \mathbf{u}^T) \right) \mathbf{V} \cdot \mathbf{n} \, ds \\
 & + \int_{\Gamma_b} \nabla \cdot \left( -\frac{\nu}{4}(\nabla \mathbf{u} + \nabla \mathbf{u}^T) : (\nabla \mathbf{u} + \nabla \mathbf{u}^T) \mathbf{V} \right) (\mathbf{W} \cdot \mathbf{n}) \, ds \\
 & + \int_{\Gamma_b} \nabla \cdot \left( -\frac{\nu}{2}(\nabla \boldsymbol{\lambda} + \nabla \boldsymbol{\lambda}^T) : (\nabla \mathbf{u} + \nabla \mathbf{u}^T) \mathbf{V} \right) (\mathbf{W} \cdot \mathbf{n}) \, ds.
 \end{aligned}$$

To obtain this final simplified form of the shape Hessian, we have used the fact that since  $\Gamma_p$  and  $\Gamma_t$  are fixed boundaries (i.e., not subject to perturbations), the normal components  $\mathbf{V} \cdot \mathbf{n}$  and  $\mathbf{W} \cdot \mathbf{n}$  of the shape perturbations have to vanish on these boundaries. Thus, one can rewrite the integral over  $\Gamma_b$  in (3.7) as an integral over  $\partial\Omega$  and apply (2.4).

We remark that, compared to the incremental state equation in [25],<sup>2</sup> the boundary condition in (3.12) contains the additional terms  $\nabla \mathbf{u}^T \mathbf{n}$  and  $\nabla \boldsymbol{\lambda}^T \mathbf{n}$ . However, using the homogeneous boundary condition for  $\mathbf{u}$  and  $\boldsymbol{\lambda}$  on  $\Gamma_b$ , as well as the divergence-free condition, one can argue that  $\nabla \mathbf{u}^T \mathbf{n} = 0$  and  $\nabla \boldsymbol{\lambda}^T \mathbf{n} = 0$ . This argument is similar to the proof of (3.8). Summarizing, we have the following theorem.

**THEOREM 3.2.** *The application of the shape Hessian operator at  $\Omega$  to directions  $(\mathbf{V}, \mathbf{W})$  is given by (3.16), where  $(\mathbf{u}, p)$  and  $(\boldsymbol{\lambda}, \alpha)$  denote the solution to the state and adjoint equations, respectively, and  $(\hat{\mathbf{u}}, \hat{p})$  and  $(\hat{\boldsymbol{\lambda}}, \hat{\alpha})$  denote the solution to the incremental state and incremental adjoint equations (3.12) and (3.15), respectively.*

**4. Couette and Poiseuille flow examples.** In this section, the shape gradient and shape Hessian given in Theorems 3.1 and 3.2 are evaluated for the special case of a flat boundary. In this case, analytical Hessians are found for Stokes flow, while only numerical Hessians are available for Navier–Stokes flow.

It will be shown below that the flat boundary is a stationary point of the roughness functional  $\mathcal{D}$ ; that is, the shape gradient vanishes. Hence, the behavior of  $\mathcal{D}$  around the flat boundary is dominated by its second-order shape derivatives, as illustrated by the Taylor expansion

$$(4.1) \quad \mathcal{D}(\Gamma_b) \approx \mathcal{D}(\Gamma_b^0) + d\mathcal{D}(\Gamma_b^0, \mathbf{V}) + \frac{1}{2}d^2\mathcal{D}(\Gamma_b^0; \mathbf{V}, \mathbf{V}),$$

where  $\Gamma_b$  is the perturbed boundary given by

$$\Gamma_b = \{\mathbf{x} : \mathbf{x} = \mathbf{X} + \mathbf{V}(\mathbf{X}) \text{ for } \mathbf{X} \in \Gamma_b^0\}.$$

Since this analysis is for a domain with fixed volume, the admissible boundary perturbations  $\mathbf{V}(\mathbf{X})$  must satisfy

$$(4.2) \quad \int_{\Gamma_b} \mathbf{V} \cdot \mathbf{n} \, ds = 0.$$

In what follows, we restrict ourselves to considering only boundary perturbations in the wall-normal direction. This assumption limits the roughness topographies we permit but enables the use of Fourier modes as a parametrization. However, it

---

<sup>2</sup>The incremental state equation is referred to as local shape derivative in [25], where it is used to derive the shape gradient.

excludes certain topographies, for instance, those that cannot be written as a single-valued function of  $x$  and  $y$ .

Due to the periodicity of the boundary perturbations in both  $x$  and  $y$ , it will be convenient to expand the boundary perturbations in a Fourier basis. To this end, the normalized one-dimensional Fourier basis in the streamwise ( $x$ ) direction is defined as

$$\psi_j^x = \frac{1}{\sqrt{L_x}} \begin{cases} 1 & \text{if } j = 0, \\ \sqrt{2} \sin(k_x(j)x) & \text{if } j > 0, \\ \sqrt{2} \cos(k_x(j)x) & \text{if } j < 0, \end{cases}$$

where  $L_x$  is the length of the computational domain in the  $x$  direction and  $k_x(j) = \frac{2\pi|j|}{L_x}$  is the wavenumber. Fourier basis functions  $\psi_j^y$  in the spanwise ( $y$ ) direction are defined similarly, with  $x$  replaced by  $y$ ,  $k_x$  replaced by  $k_y(j) = \frac{2\pi|j|}{L_y}$ , and  $L_x$  replaced by  $L_y$  (the domain size in the  $y$  direction). A basis for the boundary perturbations is then given by  $\mathbf{V}_{i,j} = (0, 0, \psi_{i,j})^T$  with  $\psi_{i,j} = \psi_i^x \psi_j^y$ , where, because the mean distance between the top and bottom walls is constrained to remain constant  $h$ , the function  $\psi_{00}$  is excluded from the basis of allowed shape perturbations. Note that for these shape perturbations  $\mathbf{V}_{i,j}$ , the condition (2.5) is satisfied, and thus the shape Hessian will be symmetric. Moreover, for  $\mathbf{V}_{i,j}$  defined above, we have  $\nabla \cdot \mathbf{V}_{i,j} = 0$ . Thus using the regularity of  $\Omega$ , the boundary data, and the forcing  $\mathbf{f}$ , we can define the following function  $h(\mathbf{W})$  on  $\Gamma_b$ :

$$\begin{aligned} h(\mathbf{W}) = & \left( -\frac{\nu}{2}(\nabla \mathbf{u} + \nabla \mathbf{u}^T) : (\nabla \hat{\mathbf{u}} + \nabla \hat{\mathbf{u}}^T) - \frac{\nu}{2}(\nabla \lambda + \nabla \lambda^T) : (\nabla \hat{\mathbf{u}} + \nabla \hat{\mathbf{u}}^T) \right. \\ (4.3) \quad & \left. - \frac{\nu}{2}(\nabla \hat{\lambda} + \nabla \hat{\lambda}^T) : (\nabla \mathbf{u} + \nabla \mathbf{u}^T) \right) \mathbf{n} \\ & + \nabla \left( -\frac{\nu}{4}(\nabla \mathbf{u} + \nabla \mathbf{u}^T + \nabla \lambda + \nabla \lambda^T) : (\nabla \mathbf{u} + \nabla \mathbf{u}^T) \right) (\mathbf{W} \cdot \mathbf{n}). \end{aligned}$$

Then, the application of the shape Hessian (3.16) to shape directions  $(\mathbf{V}, \mathbf{W})$  can be expressed as the  $L^2$ -inner product

$$d^2 \mathcal{D}(\Gamma_b; \mathbf{V}, \mathbf{W}) = \int_{\Gamma_b} h(\mathbf{W}) \cdot \mathbf{V} \, ds.$$

Moreover, due to the regularity assumptions,  $h(\mathbf{W})$  is a continuous function on  $\Gamma_b$ . The characterization of the shape Hessian for the flat boundary is greatly simplified by the following lemma.

LEMMA 4.1. *The Fourier basis functions are eigenfunctions of the Navier–Stokes shape Hessian operator at the flat boundary  $\Gamma_b$  provided the forcing  $\mathbf{f}$  and the boundary conditions on  $\Gamma_t$  are homogeneous (i.e., independent of  $x$  and  $y$ ). To be precise, in the three-dimensional case the eigenfunctions are given by  $\mathbf{V}_{i,j} \cdot \mathbf{n} = \psi_{i,j}$ , with  $(i, j) \in \mathbb{Z}^2$ , excluding  $i = j = 0$ .*

*Proof.* Homogeneity in  $x$  and  $y$  of  $\mathbf{f}$  and the boundary conditions imply that the flow is homogeneous. Thus, the velocity and any function of the velocity, in particular the shape Hessian, are homogeneous. We define the operator  $H$  that maps the normal boundary perturbations  $\psi_{i,j}$  for the flat-boundary Hessian to  $h(\mathbf{V}_{i,j})^T \mathbf{n}$ , with  $h(\mathbf{V})$  as defined in (4.3). Thus, for  $i, j, k, l \in \mathbb{Z}$ ,

$$\int_{\Gamma_b} (H(\psi_{i,j})) \psi_{k,l} = d^2 \mathcal{D}(\Gamma_b^0, \mathbf{V}_{i,j}, \mathbf{V}_{k,l}).$$

The homogeneity of the shape Hessian implies that  $H$  commutes with translations ( $H$  is said to be a *translation-invariant operator*); therefore, for any  $\psi_{i,j}$ ,

$$\tau_{x_0,y_0}(H \psi_{i,j}) = H(\tau_{x_0,y_0} \psi_{i,j}),$$

where  $\tau_{x_0,y_0}$  is the translation-by- $(x_0, y_0)$  operator; that is,  $\tau_{x_0,y_0} f(x, y) = f(x - x_0, y - y_0)$  for a function  $f$ . Note that the Fourier basis functions defined above satisfy

$$(4.4) \quad (\tau_{-x_0} \psi_i^x)(x) = \psi_i^x(x + x_0) = \begin{cases} \psi_i^x(x) \psi_{-i}^x(x_0) + \psi_{-i}^x(x) \psi_i^x(x_0) & \text{for } i > 0, \\ \psi_i^x(x) & \text{for } i = 0, \\ \psi_i^x(x) \psi_i^x(x_0) - \psi_{-i}^x(x) \psi_{-i}^x(x_0) & \text{for } i < 0. \end{cases}$$

In the remainder of the proof,  $i, j > 0$  is imposed, and negative subscripts on  $\psi$  are indicated explicitly. With this convention, (4.4) implies

$$(4.5) \quad \begin{aligned} \tau_{-x_0,-y_0} \psi_{i,j} &= \psi_{-i,-j}(x_0, y_0) \psi_{i,j} + \psi_{i,j}(x_0, y_0) \psi_{-i,-j} \\ &\quad + \psi_{-i,j}(x_0, y_0) \psi_{i,-j} + \psi_{i,-j}(x_0, y_0) \psi_{-i,j}, \end{aligned}$$

and similar relations hold for  $\psi_{\pm i, \pm j}$ ,  $\psi_{0, \pm i}$ , and  $\psi_{\pm j, 0}$ . Using the translation invariance of  $H$ , the fact that  $H \psi_{i,j}$  can be understood as a pointwise defined function and (4.5) result in

$$(4.6) \quad \begin{aligned} (H \psi_{i,j})(x_0, y_0) &= (\tau_{-x_0,-y_0} H \psi_{i,j})(0, 0) = (H(\tau_{-x_0,-y_0} \psi_{i,j}))(0, 0) \\ &= \psi_{i,j}(x_0, y_0)(H \psi_{-i,-j})(0, 0) + \psi_{-i,-j}(x_0, y_0)(H \psi_{i,j})(0, 0) \\ &\quad + \psi_{-i,j}(x_0, y_0)(H \psi_{i,-j})(0, 0) + \psi_{i,-j}(x_0, y_0)(H \psi_{-i,j})(0, 0). \end{aligned}$$

Analogously, for  $(i, -j)$  one obtains that

$$(4.7) \quad \begin{aligned} (H \psi_{i,-j})(x_0, y_0) &= \psi_{-i,-j}(x_0, y_0)(H \psi_{i,-j})(0, 0) - \psi_{i,j}(x_0, y_0)(H \psi_{-i,j})(0, 0) \\ &\quad - \psi_{-i,j}(x_0, y_0)(H \psi_{i,j})(0, 0) + \psi_{i,-j}(x_0, y_0)(H \psi_{-i,-j})(0, 0). \end{aligned}$$

Similar expressions hold for  $(-i, -j)$ ,  $(-i, j)$  and for  $(i, 0)$ ,  $(0, j)$ . Using the fact that the Hessian, and thus  $H$ , is a symmetric operator, the orthonormality of the Fourier modes, together with (4.6) and (4.7), implies

$$(H \psi_{-i,j})(0, 0) = \int_{\Gamma_b} H \psi_{i,j} \psi_{i,-j} ds = \int_{\Gamma_b} H \psi_{i,-j} \psi_{i,j} ds = -(H \psi_{-i,j})(0, 0),$$

which shows that  $(H \psi_{-i,j})(0, 0) = 0$ . Similarly, it follows that  $(H \psi_{i,-j})(0, 0) = (H \psi_{i,j})(0, 0) = 0$ , so that  $(H \psi_{i,j})(0, 0)$  is nonzero only if both subscripts are nonpositive. With this result, only one term in (4.6), (4.7), and the analogous expressions survives, yielding

$$(4.8) \quad H \psi_{\pm i, \pm j} = (H \psi_{-i,-j})(0, 0) \psi_{\pm i, \pm j}.$$

A brief computation shows that the eigenvalue equation (4.8) also holds for  $i = 0$  or  $j = 0$ , completing the proof.  $\square$

Note that Lemma 4.1 can be seen as a particular case of a general result on translation-invariant operators. In particular, in [18] it is shown that translation-invariant operators between proper  $L_p$ -spaces are convolutions, which are known to have Fourier functions as eigenfunctions. Note that the homogeneity assumption for

the flow in Lemma 4.1 is satisfied only for homogeneous boundary conditions, volume force, and flat  $\Gamma_b$ . If these conditions are not satisfied, the eigenfunctions are not known a priori. Also, observe in (4.8) that the eigenvalues for  $\psi_{i,j}$  and  $\psi_{i,-j}$  are the same, which is also observed in the examples below.

In the first three examples, the influence of roughness on Stokes flow is considered. Stokes flow is the limit case of Navier–Stokes flow as the Reynolds number tends to zero, which results in the nonlinear term  $\mathbf{u} \cdot \nabla \mathbf{u}$  vanishing. Thus, for Stokes flow, the nonlinear term and its linearizations vanish in the state, adjoint, incremental state, and incremental adjoint equations, while the expressions for the gradient (3.7) and Hessian (3.16) remain unchanged. Three of the examples below are posed in two-dimensional domains  $\Omega$ . Thus, the deformation velocity fields simplify to  $\mathbf{V}_j = (0, \psi_j^x)$ , and a result analogous to Lemma 4.1 holds.

**4.1. Two-dimensional Stokes Couette flow.** The first example is a two-dimensional Stokes Couette flow; that is, the flow is driven by the top boundary moving at constant velocity  $\mathbf{u}_0 = (U_t, 0)^T$ . Since the bottom boundary  $\Gamma_b$  is flat, the state and adjoint systems can be solved analytically on the domain  $(0, L_x) \times (0, h)$  to obtain  $\mathbf{u} = U_t/h(y, 0)^T$  and  $\boldsymbol{\lambda} = (0, 0)^T$ , with  $h$  being the distance between the two walls. Moreover, the pressure  $p$  and adjoint pressure  $\alpha$  are constant. Thus, for the shape gradient in any admissible direction  $\mathbf{V}$ , we obtain

$$d\mathcal{D}(\Gamma_b; \mathbf{V}) = -\frac{\nu U_t^2}{2h^2} \int_{\Gamma_b} \mathbf{V} \cdot \mathbf{n} \, ds = 0.$$

The shape derivative is thus zero, and the flat boundary is a stationary point of the roughness functional. Since the Fourier functions are the eigenfunctions of the shape Hessian, the Hessian can be completely determined by evaluating it for shape perturbations in directions  $\mathbf{V}_l$  and  $\mathbf{W}_j$ . The solutions to the incremental state and adjoint equations (3.12) and (3.15) can be calculated explicitly and, letting  $k = k_x(j)$ , are given by

$$\hat{\mathbf{u}} = \begin{pmatrix} -[c_1 e^{ky} - c_2 e^{-ky} + c_3(\frac{1}{k} + y)e^{ky} + c_4(\frac{1}{k} - y)e^{-ky}] \psi_j^x(x) \\ (c_1 e^{ky} + c_2 e^{-ky} + c_3 y e^{ky} + c_4 y e^{-ky}) (\psi_j^x)'(x) \end{pmatrix}, \quad \hat{\boldsymbol{\lambda}} = \begin{pmatrix} 0 \\ 0 \end{pmatrix},$$

where

$$c_1 = \frac{h U_t k^2}{2h^2 k^2 + 1 - \cosh(2kh)}, \quad c_2 = -\frac{h U_t k^2}{2h^2 k^2 + 1 - \cosh(2kh)},$$

$$c_3 = \frac{U_t k e^{-kh} [-\sinh(kh) + k h e^{kh}]}{h (2h^2 k^2 + 1 - \cosh(2kh))}, \quad c_4 = -\frac{U_t k e^{kh} [-\sinh(kh) + k h e^{-kh}]}{h (2h^2 k^2 + 1 - \cosh(2kh))}.$$

Note that the incremental solution  $\hat{\mathbf{u}}$  exponentially decays to zero in the wall-normal direction. Its scale height, which is the size of the layer in which the incremental solution is significant, is at the order of the roughness wavelength (i.e.,  $2\pi/k$ ). Evaluating (3.16), the Hessian is found to be

$$d^2\mathcal{D}(\Gamma_b; \mathbf{V}, \mathbf{W}) = \frac{S^2 \nu L_x}{h} \gamma_c(k) \delta_{jl} \quad \text{with } \gamma_c(k) = \frac{2kh(2kh - \sinh(2kh))}{1 + 2k^2 h^2 - \cosh(2kh)} > 0,$$

where  $\delta_{jl}$  is the Kronecker delta and  $S = U_t/h$ . The diagonal structure of the Hessian operator is a consequence of the Fourier modes being eigenfunctions, and  $\gamma_c(k)$  is seen

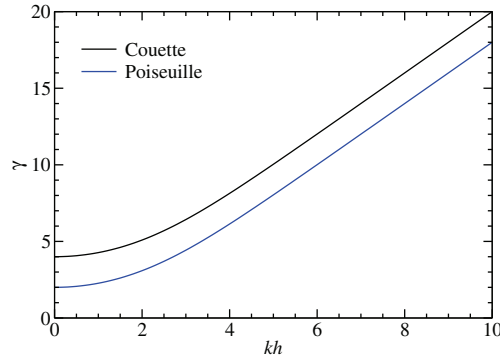


FIG. 4.1. *Eigenvalues of shape Hessian for two-dimensional Stokes flows for various frequencies  $kh$  of the shape perturbation.*

to be the scaled (i.e., dimensionless) eigenvalue associated with the Fourier mode with wavenumber  $k$ . The eigenvalues are plotted in Figure 4.1. Note that for large  $k$ ,

$$\gamma_c(k) \approx 2kh, \quad \text{where } k = 2\pi j/L_x.$$

**4.2. Two-dimensional Stokes Poiseuille flow.** Next, consider a two-dimensional Stokes Poiseuille flow (channel flow), in which no-flow conditions  $\mathbf{u}_0 = \mathbf{0}$  hold on  $\Gamma_t$  and the body force  $\mathbf{f}$  is specified such that the total mass flux through the domain  $\Omega$  is fixed, so that

$$\int_{\Omega} u_1 \, d\mathbf{x} = c, \quad \int_{\Omega} u_2 \, d\mathbf{x} = 0,$$

which implies that  $\mathbf{f} = (\frac{12c}{\nu}L_x h^3, 0)^T$ . In this case, the solutions to the state and the adjoint equations are

$$\mathbf{u} = \frac{6c}{L_x h^3} \begin{pmatrix} -y^2 + hy \\ 0 \end{pmatrix}, \quad \boldsymbol{\lambda} = \begin{pmatrix} 0 \\ 0 \end{pmatrix},$$

with constant pressure and adjoint pressure  $p$  and  $\alpha$ , respectively. The shape gradient becomes

$$d\mathcal{D}(\Gamma_b; \mathbf{V}) = -\frac{18c^2\nu}{L_x^2 h^4} \int_{\Gamma_b} \mathbf{V} \cdot \mathbf{n} \, ds = 0 \quad \text{for all admissible } \mathbf{V}.$$

Thus, again the flat boundary is a stationary point of  $\mathcal{D}$ . Also, for Poiseuille flow, the solutions to the incremental equations (3.12) and (3.15) can be derived analytically, and the application of the shape Hessian to  $\mathbf{V}_j, \mathbf{W}_l$  becomes, with  $k = k_x(j)$ ,

$$d^2\mathcal{D}(\Gamma_b; \mathbf{V}, \mathbf{W}) = \frac{S^2\nu L_x}{h} \gamma_p(k) \delta_{jl} \quad \text{with } \gamma_p(k) = \frac{2kh(2kh - \sinh(2kh))}{1 + 2k^2h^2 - \cosh(2kh)} - 2,$$

where  $S = 6c/L_x h^2$  is the gradient of the state solution on  $\Gamma_b$ . The eigenvalues for the Poiseuille case are also shown in Figure 4.1. For large  $k$ ,

$$\gamma_p(k) \approx 2kh - 2.$$

**4.3. Three-dimensional Couette flow.** The two-dimensional results from section 4.1 can be generalized to a three-dimensional Couette Stokes flow with two-dimensional roughness. The flow is driven by the boundary condition  $\mathbf{u}_0 = (U_t, 0, 0)^T$  on  $\Gamma_t$ . As in the two-dimensional case, solutions to the state and adjoint equations are found as

$$\mathbf{u} = \frac{U_t}{h} \begin{pmatrix} z \\ 0 \\ 0 \end{pmatrix}, \quad \boldsymbol{\lambda} = \begin{pmatrix} 0 \\ 0 \\ 0 \end{pmatrix}, \quad p = \text{constant}, \quad \alpha = \text{constant},$$

so that, as before, the shape gradient vanishes, making the flat wall a stationary point of the roughness functional  $\mathcal{D}$ . Solving the incremental equations as in the two-dimensional case yields, for the application of the Hessian to directions  $\mathbf{V}_{ij}$  and  $\mathbf{W}_{kl}$ ,

$$d^2 \mathcal{D}(\Gamma_b; \mathbf{V}, \mathbf{W}) = \frac{S^2 \nu L_x L_y}{h} \gamma(k_x, k_y) \delta_{ik} \delta_{jl},$$

where again the  $i$ - and  $j$ -dependence of  $k_x(i)$  and  $k_y(j)$  are not shown, and

$$\gamma(k_x, k_y) = \left(\frac{k_x}{k}\right)^2 \frac{2kh(2kh - \sinh(2kh))}{1 + 2k^2h^2 - \cosh(2kh)} + \left(\frac{k_y}{k}\right)^2 \frac{kh \cosh(kh)}{\sinh(kh)}$$

with  $k = \sqrt{k_x^2 + k_y^2}$ ,  $S = U_t/h$ . Here,  $\gamma(k_x, k_y)$  is the eigenvalue associated with wavenumber  $(k_x, k_y)$ . For large  $k$ , one obtains  $\gamma(k_x, k_y) \approx kh(1 + (k_x/k)^2)$ , and, for a constant ratio  $k_x/k_y$ ,  $\gamma_{k_x, k_y}$  increases linearly with  $k$ . Moreover, for fixed  $k$ ,  $\gamma_{k_x, k_y}$  is maximal in the case  $k_y = 0$  and minimal for  $k_x = 0$ .

Note that it is possible to obtain analytical solutions in the above examples because the incremental equations for Stokes flow can be solved analytically. To verify the above findings, the state equation was solved numerically on perturbed domains, and finite differences were used to compute the shape gradient and shape Hessian. The difference between the resulting numerically computed and the analytical eigenvalues was found to be at the order of the discretization error. More information concerning the numerical solution is provided in the Navier–Stokes example described below, where analytical solutions are not available.

**4.4. Navier–Stokes Couette flow.** Finally, consider a two-dimensional Couette flow governed by the Navier–Stokes equations. The state and adjoint equations at the flat boundary have the same solutions as for Stokes flow, namely,

$$(4.9) \quad \mathbf{u} = \frac{U_t}{h} \begin{pmatrix} y \\ 0 \end{pmatrix}, \quad \boldsymbol{\lambda} = \begin{pmatrix} 0 \\ 0 \end{pmatrix}, \quad p = \text{constant}, \quad \alpha = \text{constant}.$$

Thus, also for Navier–Stokes flow, the shape gradient vanishes at the flat boundary. Since analytical solutions to the incremental solutions are not available, the incremental equations must be solved numerically. A numerical Hessian can then be found by evaluating the expression (3.16) using the approximate solutions of the incremental equations. As proved in Lemma 4.1, the Fourier modes are the eigenfunctions of the shape Hessian for the flat boundary. This implies that, in the Fourier basis, the shape Hessian is diagonal, and hence a single pair of incremental state and incremental adjoint solves is sufficient to find all the eigenvalues. We choose  $\mathbf{W}$  as a sum of eigenfunctions (i.e., Fourier modes), solve the incremental equations, and use individual Fourier modes for  $\mathbf{V}$  in (3.16) to compute the diagonal elements of the shape Hessian.

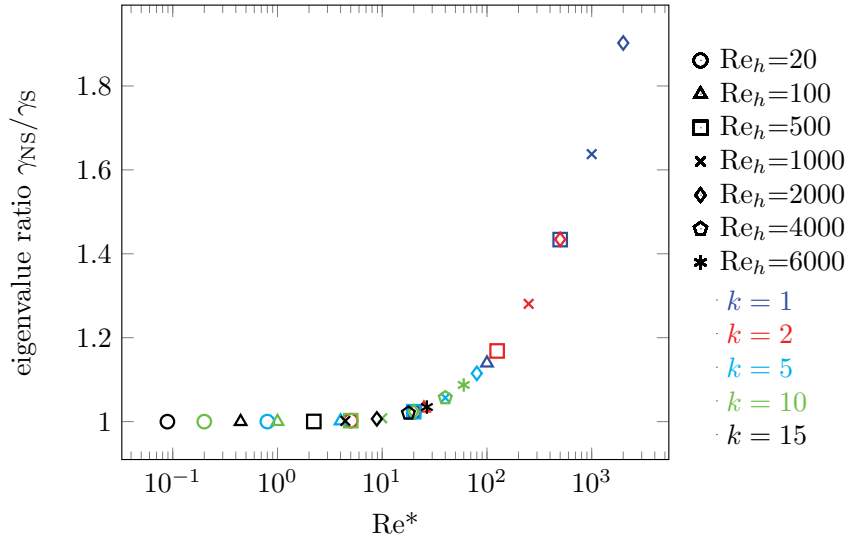


FIG. 4.2. Ratio of shape Hessian eigenvalues of Navier–Stokes and Stokes flow for the case of Couette flow. The plot shows results for  $\text{Re}_h$  ranging between 20 and 6000.

To obtain numerical solutions to the incremental state and incremental adjoint equations, the computational domain,  $\Omega$  ( $= [0, L_x] \times [0, h] \times [0, L_z]$ ), is discretized with hexahedral  $Q_4$ – $Q_2$  finite elements (i.e., biquartic polynomials represent the components of the incremental velocities  $\hat{\mathbf{u}}, \hat{\boldsymbol{\lambda}}$ , and biquadratic elements represent the incremental pressures  $\hat{p}, \hat{q}$ ). The mesh is graded towards the bottom boundary to resolve boundary layer effects. To ensure accuracy of the numerical solution, empirical convergence studies were performed using a hierarchy of meshes and an escalation of polynomial order of the finite element approximation. We found that a (graded) mesh with  $100 \times 100$  elements gives highly accurate results for the Reynolds numbers considered.

The results of these computations show that the shape Hessian eigenvalues, and thus the sensitivity of the roughness functional to Fourier basis perturbations, increase with the Reynolds number based on  $h$ , i.e.,  $\text{Re}_h = U_t h / \nu$ . For modes for which  $kh > 2\pi$ , so that the scale height of the Stokes incremental solutions (which is order  $2\pi/k$ ) is small compared to the fluid layer thickness  $h$ , the shape Hessian eigenvalues for different wavenumbers and Reynolds numbers can be made to collapse on a single curve. In fact, the ratio of the Navier–Stokes shape Hessian eigenvalues  $\gamma_{NS}$  to those for Stokes flow  $\gamma_S$  depends only on the Reynolds number  $\text{Re}^*$ ,

$$(4.10) \quad \text{Re}^* := \frac{U_t \lambda^2}{\nu h} = \text{Re}_h \frac{\lambda^2}{h^2},$$

where  $\lambda = 2\pi/k$  is the wavelength of the roughness Fourier mode. The wavelength is also the scale height of the incremental solution, so  $\text{Re}^*$  is the Reynolds number based on the scale height  $\lambda$  and on the velocity  $\lambda dU/dz = \lambda U_t/h$  at the scale height. This collapse of the ratios between Stokes and Navier–Stokes eigenvalues when plotted against  $\text{Re}^*$  is shown in Figure 4.2. Additionally, the plot shows that  $\text{Re}^*$  determines the range in which the Stokes eigenvalues are a good approximation for the Navier–Stokes eigenvalues and how they relate as  $\text{Re}^*$  increases.

Further insight into this behavior of the eigenvalues can be gained from scaling

analysis. At distances from the wall greater than the scale height  $\lambda$ , the incremental solutions decay exponentially to zero. Thus the incremental solutions are insensitive to features of the state solution farther from the wall than  $\sim \lambda$ . If  $\lambda/h$  is sufficiently small, then the incremental solutions will not depend on  $U_t$  or  $h$  separately. Instead, the only property of the state solution on which the incrementals can depend is the velocity gradient  $S = dU/dz = U_t/h$ . The incremental solutions, and therefore the Hessians, can thus depend only on three dimensional parameters ( $S$ ,  $\lambda$ , and  $\nu$ ), so by dimensional analysis, the nondimensional Hessian eigenvalues ( $\gamma_{NS}/\gamma_S$ ) depend only on the dimensionless parameter  $S\lambda^2/\nu = \text{Re}^*$ . The same argument holds in other flows (e.g., Poiseuille flow), provided that the scale height of the incremental solution is small compared to flow features in the state solution.

The Reynolds number  $\text{Re}^*$  can also be interpreted in terms of the wall scaling commonly used in the analysis of wall-bounded turbulent flows; see, e.g., [23]. In this scaling, the *wall* or *friction velocity*  $u_\tau$  is defined by  $u_\tau^2 = \nu dU/dz = \nu U_t/h$ , and the *viscous length scale*  $\delta_\nu$  is defined as  $\delta_\nu = \nu/u_\tau$ . The Reynolds number (4.10) is then given by  $\text{Re}^* = (\lambda^+)^2$ , where  $\lambda^+ = \lambda/\delta_\nu$  is the wavelength (and thus also the scale height) normalized by the viscous length scale. Since  $\lambda^+ = u_\tau \lambda/\nu$ , it can also be understood as a local Reynolds number based on  $u_\tau$  and  $\lambda$ , which measures the importance of inertial effects in the incremental solution, relative to viscous effects.

**5. Discussion.** In this paper, shape calculus is used to study the response of fluid flows to boundary roughness, particularly the response of the drag. Shape derivatives are evaluated for a flat boundary to characterize the roughness effect in the limit of small roughness. As expected, the analysis shows that the flat boundary is a stationary point of the roughness functional, so that the shape Hessian provides the lowest order description of the roughness effect. Furthermore, for a flat wall, the shape Hessian operator is translation invariant, so that its eigenfunctions are known a priori to be the Fourier functions. This allows the shape Hessian to be completely characterized by its eigenvalue spectrum and greatly simplifies the determination of the Hessian. The analysis reported here leads to the following observations regarding the sensitivity of the drag to roughness:

- The simple structure of the shape Hessian for Stokes flow allows the sensitivity of  $\mathcal{D}$  to a general small-amplitude roughness to be determined easily from the roughness spectrum. Consider a two-dimensional channel with roughness

$$\mathbf{V} \cdot \mathbf{n} = \sum_k (\alpha_k \sin(kx) + \beta_k \cos(kx))$$

satisfying

$$(5.1) \quad \sum_k \alpha_k^2 + \beta_k^2 < \infty \quad \text{and} \quad \sum_k (\alpha_k^2 + \beta_k^2)k < \infty.$$

Then, the drag increment due to this roughness is simply

$$(5.2) \quad \delta \mathcal{D} = \frac{L_x S^2 \nu}{2h} \sum_k (\alpha_k^2 + \beta_k^2) \gamma(k).$$

Due to the assumption (5.1) and the fact that  $\gamma(k) \approx 2hk$  for large  $k$ , the sum in (5.2) converges. While valid only for small roughness heights, this is nonetheless a useful result, as it provides a simple metric for the effect of roughness surface topography on the drag, and (4.1) (or (5.2)) applies

to all roughnesses that are Lipschitz continuous and satisfy condition (5.1). The expression (5.2) also applies to the roughness analysis for Navier–Stokes flow with the Stokes Hessian eigenvalues  $\gamma(k)$  replaced by the Navier–Stokes Hessian eigenvalues. The latter are well approximated by  $\gamma(k)$  if  $\text{Re}^*$  (as defined in (4.10)) is small; see Figure 4.2.

- For all  $k$ ,  $\gamma_c(k) > 0$  and  $\gamma_p(k) > 0$ . Since all Hessian eigenvalues are positive, the flat boundary corresponds to a local minimum of the roughness functional. Moreover, for Stokes flow it is the global minimum, since the flat boundary is the only stationary point. This is due to the fact that  $d\mathcal{D}(\Gamma_b; \mathbf{V})$  vanishes if and only if  $\nabla \mathbf{u}$  is constant on  $\Gamma_b$  with  $\boldsymbol{\lambda} = 0$  for Couette flow and  $\boldsymbol{\lambda} = -\mathbf{u}$  for Poiseuille flow, and the flat boundary is the only shape for which this is true.
- In Stokes flow, for large wavenumbers ( $kh > 2\pi$ ),

$$\gamma_c(k) \approx 2kh, \quad \gamma_p(k) \approx 2kh - 2,$$

which shows that the eigenvalues increase linearly with the wavenumber. Thus, the sensitivity of the roughness functional increases linearly with the wavenumber of the boundary perturbation. Provided  $hk \gg 1$ , that is, the height ( $h$ ) of the channel is much larger than the scale height of the incremental solution,

$$\gamma_c(k) \approx \gamma_p(k) \approx 2kh.$$

In this case, the boundary conditions on the far outer flow do not influence the flow increment due to the roughness.

- The linear dependence of the eigenvalues with the wavenumber shows that the Hessian for Stokes flow is a pseudodifferential operator with order 1. This is also pointed out in [25], where the Hessian operator is considered as an input-to-output mapping in frequency space, which is motivated by the derivation of operator symbols.
- For small  $k$ ,  $\gamma(k)$  approaches the asymptotic value of 4 or 2 for Couette or Poiseuille flow, respectively. When  $kh \ll 1$ , the scale height of the incremental solution is much larger than the fluid layer. The solution details in this case thus depend on the boundary conditions on the upper surface.
- For Navier–Stokes Couette flow, the flat boundary also corresponds to a stationary point of  $\mathcal{D}$  (a minimum). The sensitivity of the roughness functional to Fourier basis perturbations increases with the Reynolds number. The ratio of the Navier–Stokes shape Hessian eigenvalues to those for Stokes flow depends only on the Reynolds number  $\text{Re}^*$  (as defined in (4.10)), which can be understood using scaling arguments.
- The scaling arguments mentioned above (see section 4.4) also provide guidance for the applicability of the Navier–Stokes Couette flow analysis to roughness in a turbulent wall layer. For the analysis to apply, the scale height of the incremental solutions (of order  $\lambda$ ) must not exceed the sublayer thickness, which is approximately  $5\delta_v$  [23]. Therefore, of the results shown in Figure 4.2, only those with  $\text{Re}^* < 25$  ( $\lambda^+ < 5$ ) are a valid approximation for turbulent flows.

Finally, note that roughness is of particular concern in turbulent flows. A particularly useful generalization of the steady Navier–Stokes shape Hessian analysis would

thus be its application to turbulence. This would require generalization to the time-dependent Navier–Stokes state equation, and the definition of the drag functional as a time average.

## REFERENCES

- [1] Y. ACHDOU, O. PIRONNEAU, AND F. VALENTIN, *Effective boundary conditions for laminar flows over periodic rough boundaries*, J. Comput. Phys., 147 (1998), pp. 187–218.
- [2] R. A. ADAMS, *Sobolev Spaces*, Academic Press, New York, 1975.
- [3] A. ALMQVIST, E. ESSEL, J. FABRICIUS, AND P. WALL, *Variational bounds applied to unstationary hydrodynamic lubrication*, Internat. J. Engrg. Sci., 46 (2008), pp. 891–906.
- [4] A. ALMQVIST, E. ESSEL, L.-E. PERSSON, AND P. WALL, *Homogenization of the unstationary incompressible Reynolds equation*, Tribology International, 40 (2007), pp. 1344–1350.
- [5] E. ARIAN, *Analysis of the Hessian for Aerodynamic Optimization*, Technical report, Institute for Computer Applications in Science and Engineering (ICASE), Hampton, VA, 1995.
- [6] E. ARIAN AND S. TA’ASAN, *Analysis of the Hessian for Aerodynamic Optimization: Inviscid Flow*, Technical report, Institute for Computer Applications in Science and Engineering (ICASE), Hampton, VA, 1996.
- [7] J. CÉA, *Numerical methods of shape optimal design*, in Optimization of Distributed Parameter Structures, Vol. II, J. E. J. Haug, ed., Sijthoff and Noordhoff, Alphen ann den Rijn, The Netherlands, 1981, pp. 1049–1087.
- [8] H. CHOI, P. MOIN, AND J. KIM, *Direct numerical simulation of turbulent flow over riblets*, J. Fluid Mech., 255 (1993), pp. 503–539.
- [9] M. C. DELFOUR AND J.-P. ZOLÉSIO, *Velocity method and Lagrangian formulation for the computation of the shape Hessian*, SIAM J. Control Optim., 29 (1991), pp. 1414–1442.
- [10] M. C. DELFOUR AND J.-P. ZOLÉSIO, *Shapes and Geometries: Analysis, Differential Calculus, and Optimization*, Adv. Des. Control 4, SIAM, Philadelphia, 2001.
- [11] K. EPPLER AND H. HARBRECHT, *A regularized Newton method in electrical impedance tomography using shape Hessian information*, Control Cybernet., 34 (2005), pp. 203–225.
- [12] K. EPPLER AND H. HARBRECHT, *Second-order shape optimization using wavelet BEM*, Optim. Methods Softw., 21 (2006), pp. 135–153.
- [13] K. EPPLER, S. SCHMIDT, V. SCHULZ, AND C. ILIC, *Preconditioning the pressure tracking in fluid dynamics by shape Hessian information*, J. Optim. Theory Appl., 141 (2009), pp. 513–531.
- [14] L. C. EVANS, *Partial Differential Equations*, American Mathematical Society, Providence, RI, 1998.
- [15] M. D. GUNZBURGER, *Perspectives in Flow Control and Optimization*, Adv. Des. Control 5, SIAM, Philadelphia, 2002.
- [16] H. HARBRECHT, *Analytical and numerical methods in shape optimization*, Math. Methods Appl. Sci., 31 (2008), pp. 2095–2114.
- [17] M. HINTERMÜLLER AND W. RING, *An inexact Newton-CG-type active contour approach for the minimization of the Mumford-Shah functional*, J. Math. Imaging Vision, 20 (2004), pp. 19–42.
- [18] L. HORMANDER, *Estimates for translation invariant operators in  $L_p$  spaces*, Acta Math., 104 (1960), pp. 93–140.
- [19] K. ITO AND K. KUNISCH, *Lagrange Multiplier Approach to Variational Problems and Applications*, Adv. Des. Control 15, SIAM, Philadelphia, 2008.
- [20] W. JÄGER AND A. MIKELIĆ, *On the roughness-induced effective boundary conditions for an incompressible viscous flow*, J. Differential Equations, 170 (2001), pp. 96–122.
- [21] J. LIONS, *Optimal Control of Systems Governed by Partial Differential Equations*, Springer-Verlag, Berlin, Heidelberg, New York, 1971.
- [22] B. MOHAMMADI, O. PIRONNEAU, AND F. VALENTIN, *Rough boundaries and wall laws*, Internat. J. Numer. Methods Fluids, 27 (1998), pp. 169–177.
- [23] S. POPE, *Turbulent Flows*, Cambridge University Press, Cambridge, UK, 2000.
- [24] M. PRAT, F. PLOURABOUÉ, AND N. LETALLEUR, *Averaged Reynolds equation for flows between rough surfaces in sliding motion*, Transport in Porous Media, 48 (2002), pp. 291–313.
- [25] S. SCHMIDT AND V. SCHULZ, *Impulse response approximations of discrete shape Hessians with application in CFD*, SIAM J. Control Optim., 48 (2009), pp. 2562–2580.
- [26] J. SOKOŁOWSKI AND J.-P. ZOLÉSIO, *Introduction to Shape Optimization. Shape Sensitivity Analysis*, Springer Ser. Comput. Math. 16, Springer-Verlag, Berlin, 1992.
- [27] R. TEMAM, *Navier Stokes Equations. Theory and Numerical Analysis*, North–Holland, Amsterdam, New York, Oxford, 1979.

- [28] R. TEMAM, *Navier–Stokes Equations and Nonlinear Functional Analysis*, 2nd ed., CBMS-NSF Regional Conf. Ser. in Appl. Math. 66, SIAM, Philadelphia, 1995.
- [29] F. TRÖLTZSCH, *Optimal Control of Partial Differential Equations: Theory, Methods and Applications*, Grad. Stud. Math. 112, American Mathematical Society, Providence, RI, 2010.
- [30] M. J. WALSH, *Riblets as a viscous drag reduction technique*, AIAA J., 21 (1983), pp. 485–486.
- [31] J. P. ZOLÉSIO, *Identification de domaines par déformation*, Ph.D. thesis, Université de Nice, Nice, France, 1979.